Profiling the diversity of agonist-selective effects on the proximal proteome environment of G protein-coupled receptors

Benjamin J. Polacco[1,2,3]*, Braden T. Lobingier[4]*, Emily E. Blythe[1,3,5], Nohely Abreu[6], Jiewei Xu[1,2,3], Qiongyu Li[1,2,3], Zun Zar Chi Naing[1,2,3], Brian K. Shoichet[1,7], Joshua Levitz[6], Nevan J. Krogan[1,2,3], Mark Von Zastrow[1,3,5$], Ruth Hüttenhain[1,2,3$]

[1]Quantitative Biosciences Institute (QBI), University of California, San Francisco, San Francisco, CA, USA.
[2]J. David Gladstone Institutes, San Francisco, CA, USA.
[3]Department of Cellular and Molecular Pharmacology, University of California, San Francisco, San Francisco, CA, USA.
[4]Department of Chemical Physiology and Biochemistry, Oregon Health and Sciences University, Portland, Oregon, USA.
[5]Department of Psychiatry and Behavioral Sciences, University of California, San Francisco, San Francisco, CA, USA.
[6]Department of Biochemistry, Weill Cornell Medicine, New York, NY, USA.
[7]Department of Pharmaceutical Chemistry, University of California, San Francisco, San Francisco, CA, USA.
*Authors contributed equally
[$]Co-corresponding authors

Abstract

G protein-coupled receptors (GPCRs) regulate many aspects of physiology and represent actionable targets for drug discovery. These receptors translate ligand-dependent input into a cellular response by remodeling protein interaction networks that are exquisitely organized both spatially and temporally. APEX-based proximity biotin labeling combined with quantitative mass spectrometry has emerged as a powerful approach for capturing all aspects of this dynamic ligand-dependent cellular re-organization. However, a major challenge in this approach is the extraction of salient information from these highly complex datasets. Here, we describe a computational framework for analyzing proximity labeling datasets that reliably predicts the subcellular location of GPCRs and deconvolutes spatial and temporal components of protein interaction network organization. Focusing on the mu-opioid receptor and its activation with distinct agonist drugs, we demonstrate the applicability of this framework to resolve agonist-specific differences in receptor localization and trafficking as well as the protein interaction networks it engages. Using this approach, we discover two novel protein network components which produce widespread, yet distinct, effects on G protein-dependent signaling. While the framework is broadly applicable to proximity biotin labeling datasets, it holds specific promise for further rationalizing GPCR drug discovery efforts by providing an unbiased assessment of ligand-dependent effects, and by enabling the discovery of additional network components for consideration as novel therapeutic targets.

Introduction

G protein-coupled receptors (GPCRs) regulate a diverse array of intracellular signaling cascades in response to hormones, neurotransmitters, ions, odorants and other stimuli. As such, they play an essential role in physiology and disease. Additionally, they represent the largest family of membrane targets for US Food and Drug Administration (FDA)-approved drugs.[1] Activation of GPCRs initiates complex signaling networks through heterotrimeric G proteins and G-protein-independent pathways mediated by arrestin coupling and other effectors.[2,3] Activation of GPCR-mediated signaling pathways is commonly assessed by measuring (1) the engagement of selected signal transducers such as G proteins[4,5] and β-arrestins, (2) the levels of second messengers including cAMP[6] or Ca^{2+}, or (3) the modulation of ion channel activity. While these approaches are robust and in part scalable to screen libraries of novel putative ligands, they mostly measure selected binary interactions between a GPCR and a signal transducer, but do not provide information about the cellular location of the receptor or the interaction networks that regulate receptor activity. This information is crucial as GPCRs dynamically traffic through multiple cellular organelles and can engage organelle-specific proteins during this process.[7] Notably, GPCRs can activate signaling cascades from these intracellular membranes,[8–12] underscoring the spatio-temporal complexity of these therapeutically relevant signaling proteins.

Depending on the cellular location and the signaling pathways activated, GPCRs can elicit different cellular effects.[13,14] This capacity may be exploited in drug discovery by designing ligands that selectively activate specific receptor-mediated signaling pathways[15–17] or target receptors at selected cellular locations.[18–20] Such approaches have the potential to provide therapeutic actions with fewer deleterious side effects. However, efforts to create pathway or location specific ligands are limited by our understanding of GPCR-based signaling and trafficking mechanisms. The mu opioid receptor (MOR) is a well-studied example of how structurally distinct agonists evoke different spatio-temporal responses. Highly efficacious agonists, such as the endogenous peptide agonist or fentanyl, cause strong signaling and efficient receptor trafficking.[21] In striking contrast, less efficacious agonists have been reported to cause minimal receptor trafficking, reduced signaling, and changes to signaling location or regulatory mechanisms.[11,21] Thus, some opiate alkaloids and synthetic opioids have the potential to elicit distinct spatio-temporal effects compared to endogenous peptide agonists but identifying the myriad of molecular changes has been challenging. One reason for this is the lack of technologies that can capture the full complexity of ligand-evoked GPCR activity.

Recently, we and others established GPCR-APEX, a proximity biotin labeling method for GPCRs based on an engineered ascorbic acid peroxidase (APEX) fused to the receptor[22,23] combined with quantitative mass spectrometry (MS).[24,25] We demonstrated that GPCR-APEX simultaneously captures proximal protein interaction networks and cellular location of the activated receptor in an unbiased manner and with high temporal resolution through the quantification of thousands of proteins that are biotinylated proximal to the receptor following activation. While this represents a powerful method to profile agonist-selective effects on receptor activation, a major limitation of its application has been to deconvolve information about interaction networks and receptor location from these proximity labeling datasets.[24] Here, we developed a novel computational framework which (1) predicts time and agonist dependent subcellular location of the receptor by utilizing a system of spatially specific APEX references and

(2) quantitatively deconvolutes the effect of receptor location and proximal interactors in the proximity labeling data.

As our model system for developing the framework, we selected MOR given its pharmacologic relevance, the availability of several distinct ligands targeting the receptor, and the recent evidence that it signals by engagement of transducer proteins at different cellular locations.[7,11] Upon activating MOR with the chemically distinct agonists DAMGO, morphine, and PZM21, we show pronounced differences in the proximal proteome of MOR elicited by their distinct capacity to initiate receptor trafficking as predicted by our framework. The trafficking behavior of the receptor upon activation was directly correlated with the engagement of interactors, such as β-arrestins. In addition to defining these agonist-specific effects, we discovered two novel G protein associated proteins, EYA4 and KCTD12, which were detected in the MOR proximal proteome and which regulate G protein signaling in distinct ways, apparently by interacting directly with and buffering dissociated G protein subunits.

Results

Proximal proteome changes of MOR activated by diverse ligands are driven primarily by differences in subcellular location

We first sought to use our approach combining APEX-based proximity biotin labeling and quantitative MS to investigate, in an unbiased manner, how structurally distinct opioids control the proximal proteome environment of MOR.[24] Three agonists, DAMGO, morphine, and PZM21[15] were chosen to represent distinct chemistries as well as different efficacies and cellular responses to receptor activation. DAMGO is a peptide full agonist which causes strong activation of both G protein and β-arrestin pathways.[26] Morphine represents a naturally occurring alkaloid and partial agonist for both G protein and β-arrestin pathways.[26,27] PZM21 is a synthetic MOR agonist unrelated to classic morphinans, which exhibits strong partial agonism for G protein activation and negligible activation of the β-arrestin pathway.[15] First, we stably expressed the receptor-APEX fusion construct in HEK293 cells, which retained receptor function with regard to signaling, internalization, and recycling (**Figure S1**). To perform proximity labeling, the cells were pretreated with biotin-phenol followed by activation of MOR using DAMGO, morphine, or PZM21 at a concentration of 10μM over a time course of up to 60 minutes (**Figure 1A**). At selected time points after receptor activation, we initiated proximal biotin labeling by addition of hydrogen peroxide (H_2O_2) for 30 seconds, followed by quenching of the reaction, cell lysis, and enrichment of biotinylated proteins using streptavidin. To quantify relative abundance changes of biotin-labeled proteins after agonist stimulation, we utilized a combination of quantitative proteomics approaches encompassing unbiased proteomics as well as targeted proteomics based on selected reaction monitoring (SRM).

We next asked how the proximal protein environment of the receptor globally changes in a ligand-dependent manner (**Figure 1B**). To this end, we performed a statistical analysis determining proteins with significant changes in biotin labeling over the time course. For each observed protein and ligand, we scored changes in biotin labeling by fitting the time course with a polynomial curve and performed an F-test comparing it against a model with no time term. We then calculated a single significance score for each protein and ligand that summarizes the confidence, strength,

and direction of the biotin labeling changes by combining the maximum fold change over the time course as a measure of strength and direction with the p-value as a measure for confidence (see **Methods** and **Table S1**). Following hierarchical clustering of the significant proteins based on their significance score across the three ligands, we performed gene ontology (GO) enrichment analysis for each cluster.

This unbiased view of the agonist dependent proximal protein environment of MOR indicated that (1) the majority of changes in biotin-labeled proteins are evoked by receptor endocytosis and trafficking and (2) the three ligands differ strongly in their capacity to induce endocytosis and trafficking (**Figure 1B, Figure S2**). To assess ligand-dependent receptor localization quantitatively, selected localization markers for plasma membrane, early endosome and late endosome/lysosome were monitored using targeted proteomics (**Table S2**). We observed that DAMGO shifted the distribution of MOR from the plasma membrane to endosomes and lysosome, while morphine resulted in less endocytosis and, astonishingly, PZM21 led to no detectable changes in MOR localization at the plasma membrane at all, something perhaps consistent with the functional selectivity for which it was developed[15] (**Figure 1C**). Together these data underscore how structurally distinct ligands can strongly influence the subcellular location of a receptor and highlight the need for a systematic approach to identify the location-specific proximal proteome(s).

Computational framework to predict ligand-dependent receptor trafficking

We recently introduced a system of spatially specific APEX-references, i.e. APEX constructs that are localized to selected subcellular compartments. Fusing the enzyme to protein localization domains or compartment-specific proteins allowed us to determine the proteome of a subcellular compartment.[24] These control conditions enabled us to begin to deconvolve the complex proteomic profiles captured by GPCR-APEX into (1) spatial bystanders, i.e. location-specific proteins that reside in the local environment of the receptor but do not physically interact or directly participate in its function and (2) proximal protein networks that can regulate receptor signaling and trafficking. However, a challenge to this approach is that over longer timescales proteins, such as GPCRs, can traffic to many different compartments. Thus, the question arising is: how can the complex localization be quantitatively determined so that the correct spatial controls can be applied in the appropriate proportions?

As demonstrated in our previous study, proteins captured in the proximity labeling data can be used to infer information about the subcellular location of the receptor.[24] To quantitatively model receptor location across multiple subcellular compartments, we first selected relevant spatial references for the plasma membrane (PM-APEX), early endosome (Endo-APEX), and lysosome (Lyso-APEX) (**Figure 2A**), which were processed in parallel with the MOR proximity labeling samples. We then determined indicative proteins for subcellular locations by pairwise comparison of the biotin labeling data from the three spatial references using statistical models implemented in MSstats.[28] All proteins were considered location indicators which (1) showed a p-value below 0.005 and a log2 fold change (Log2FC) higher than 1.0 for at least one of the comparisons and (2) were required to be consistently quantified across all replicates above a certain intensity threshold (**Figure 2B**, **Table S3**). Next, we used these indicator proteins to quantitatively estimate

the ligand-dependent fraction of the receptor at a given cellular location across the time course. Specifically, we calculated location coefficients for each ligand, time point and biological replicate by solving a linear model based on the protein intensities of the location indicators across the spatial references and across the receptor APEX samples (**Figure 2C**). The model-based cellular location coefficients for the receptor accurately recapitulated the relative locations determined experimentally by the targeted proteomics measurements (**Figure 1C**), suggesting that our computational framework is very powerful in predicting receptor trafficking.

Proteins regulating receptor function are enriched around the GPCR through interaction networks and can thus be quantitatively distinguished from the spatial bystanders by comparing the GPCR-APEX sample to the location-dependent background proteome.[24] We next tested whether we could leverage the model-based coefficients to deconvolve the two time-dependent profiles of spatial bystanders and proximal protein interaction networks. To this end, we calculated for all proteins in the dataset expected intensities based on the cellular location changes of the receptor. Therefore, we combined the location coefficients for each ligand, time point and biological replicate and the intensities of all proteins quantified across the PM, Endo, and Lyso-APEX spatial references (**Figure 2D, Figure S3**). Finally, based on the assumption that observed protein intensities are a combination of both GPCR proximal interaction networks and spatial bystanders, we detrended the observed protein intensities for each ligand, timepoint and replicate combination with the spatially-expected protein intensities. In brief, a protein's expected log-intensity, based on spatial references and ligand/time-specific coefficients, was subtracted from its observed log-intensity to produce a detrended log-intensity (**Table S4**). On the example of EEA1, a spatial bystander of MOR at the early endosome, we demonstrated that detrending the data allows to account for the increase in biotin labeling after activation of the receptor with DAMGO and morphine (**Figure 2E**, right panel). In contrast, the agonist-dependent temporal profiles for ARRB2 (**Figure 2E**, left panel), a protein that is recruited to the receptor upon activation and known to regulate receptor trafficking and signaling, as well as members of the AP2 complex (**Figure S4**), which directs the receptor/β-arrestin complexes into clathrin-coated pits, were not affected by the detrending.

The final outcome of the novel computational framework is the prediction of ligand-specific receptor trafficking directly from the proximity labeling data in contrast to measuring it independently with complementary methods. The advantage of such approach is that it requires minimal knowledge of receptor trafficking itinerary and its kinetics. Simultaneously, the framework can subtract location-specific trends from the GPCR-APEX datasets to enrich functionally relevant proteins that reside in the proximal interaction network of the receptor.

EYA4 and KCTD12 are novel G-protein dependent factors recruited in the proximal interaction network of MOR

After detrending the proximity labeling dataset to account for labeling of spatial bystander proteins, we sought to identify putative novel proteins in the proximal interaction network regulating MOR function. To this end we performed statistical analysis on the detrended protein intensities by fitting the time course with a polynomial curve and performing an F-test to compare it against a model with no time term. All proteins with significant changes in biotinylation

(Log2FC>1 and p-value<0.001) before and after data detrending for at least one ligand were considered part of the proximal interaction network of MOR and were clustered based on their significance score across the three ligands (**Figure 3A, Table S5**).

We observed that DAMGO evoked the majority of significant changes in the proximal interaction network, including proteins known to regulate receptor endocytosis and receptor trafficking (**Figure S5**). Conversely, the proximal interaction network of the receptor showed only a few changes when activated with PZM21 (**Figure 3A**). Rather than engaging different proteins, our data suggests that the proximal interaction networks of MOR activated by morphine and PZM21 represent a subset of the DAMGO network likely differing in interactors involved in receptor endocytosis and trafficking. As an example, ARRB2 showed a strong increase in biotin labeling upon activation of MOR with DAMGO; in contrast, activation by morphine showed less recruitment of ARRB2, and activation by PZM21 did not elicit a visible change in biotin labeling of ARRB2, again consistent with its original design[15] (**Figure 3B**). Notably, ligand-dependent changes in ARRB2 biotin labeling were correlated with the degree of MOR endocytosis as predicted by the location coefficients (**Figure 3C, Figure S6**), which is consistent with previous findings.[21]

Despite the observed ligand-dependent differences in the MOR proximal interaction network, we discovered two proteins, EYA4 and KCTD12, showing an increase in biotin labeling upon receptor activation with all ligands (**Figure 3B**). EYA4 belongs to the family of Eyes absent (EYA) proteins consisting of the four paralogs EYA1-EYA4, which represent multifunctional proteins containing phosphothreonine and phosphotyrosine phosphatase activity as well as transcriptional co-activator function when tethered to DNA through interaction with the SIX (sine oculis) family of homeodomain proteins.[29] Interestingly, prior studies have shown that another member of the EYA family, EYA2, can interact and colocalize with constitutively active Gαi proteins[30,31] mediating an attenuation of cAMP inhibition.[31] KCTD12 has been well characterized as auxiliary subunit for the $GABA_B$ receptor regulating the rise time and duration of G protein-coupled inwardly rectifying potassium channels (GIRKs)[32,33] by competing with GIRK binding to the released Gβγ subunit and thus rapidly stripping Gβγ subunits from the activated channel, resulting in channel closure.[34]

Based on the prior knowledge and the fact that EYA4 and KCTD12 were labeled by all three MOR agonists including those which stimulate negligible trafficking, we hypothesized that both proteins might regulate G protein signaling downstream of MOR. Indeed, a proximity labeling experiment of the plasma membrane (PM-APEX) upon activation of MOR with DAMGO in the presence and absence of the $G_i\alpha$ inhibitor pertussis toxin (PTX) validated that the recruitment of KCTD12 and EYA4 to the plasma membrane is not only dependent on MOR activity, but also on $G_i\alpha$ activity (**Figure 4A,B**). Interestingly, PTX treatment in the absence of MOR activation decreased biotin labeling of EYA4 at the plasma membrane significantly (log2FC -1.0, p-value $2x10^{-8}$, **Figure 4B**), suggesting that EYA4 might already be bound to a certain extent to $G_i\alpha$ before MOR activation. Indeed, when we performed purifications of affinity-tagged EYA4 we detected its interaction with $G_i\alpha$ proteins at basal levels in addition to known interactors including SIX proteins (**Figure 4C**). Moreover, we found that introduction of the A633R SIX-binding mutation interfered with interaction of both $G_i\alpha$ and SIX proteins, while the D375N phosphatase-dead mutant did not alter the interactions significantly (**Figure 4C**). Finally, APEX-based proximity labeling for EYA4 indicated

an increase in labeling of plasma membrane and a decrease in labeling of nuclear proteins, which was dependent on $G_i\alpha$ activity (**Figure 4D,E, Figure S7**).

Taken together, our data suggest that EYA4 and KCTD12 are recruited in the proximity of MOR in a receptor and $G_i\alpha$ activity-dependent manner, and thus might function as regulators of MOR signaling through G proteins. However, based on the previously discovered function of KCTD12[34] and our experimental data for EYA4, we hypothesize that these regulatory proteins do not engage the receptor itself, but rather interact with the $G\beta\gamma$ and $G_i\alpha$ subunits, respectively, that are released by dissociation of the heterotrimeric G protein upon MOR activation.

EYA4 and KCTD12 modulate functional signaling through G proteins

As our results indicate that EYA4 interacts with $G_i\alpha$ subunits (**Figure 4C**) and KCTD12 was previously established to bind $G\beta/\gamma$ subcomplexes,[32,33] we focused on cellular G protein signaling for initial functional assessment. We began by assaying signaling through cytoplasmic cAMP production. GPCRs stimulate or inhibit cAMP production by coupling to $G_s\alpha$ and $G_i\alpha$, respectively. Using isoproterenol to activate endogenous $G_s\alpha$-coupled β-adrenergic receptors in HEK293 cells, we verified the characteristic $G_s\alpha$-mediated cAMP response as defined by elevation of cAMP to a peak within several minutes followed by a decrease or desensitization phase in the prolonged presence of agonist (**Figure 5A left**, black curve). Using DAMGO to activate exogenously expressed MOR (blue) or somatostatin (SST) to activate endogenous $G_i\alpha$-coupled somatostatin (SST) receptors (green) in HEK293 cells, we verified inhibition of the cAMP response throughout its time course and affecting the time-integrated response (**Figure 5A right**). DAMGO inhibited the response more strongly than SST, consistent with recombinant MOR being overexpressed.

We then applied the cAMP assay to investigate effects of EYA4 and KCTD12. Depleting endogenous EYA4 by CRISPR-mediated gene knockout (EYA4 KO, **Figure S8**) suppressed the isoproterenol-induced cAMP response over its full time course (**Figure 5B left**, open circles), resulting in a significant reduction of the integrated cAMP response (**Figure 5B right**). A similar effect was observed in an independent KO cell clone (**Figure S9A**). The magnitude of inhibition was comparable to that produced by SST in control (non-targeting, or NT) cells (compare **Figure 5A** and **B**), suggesting that this effect is in a functionally relevant range, and GPCR activation was able to further suppress the signal (**Figure 5C, Figure S9B**).

KCTD12 KO did not detectably change the peak cAMP response but produced an apparent slowing of desensitization. This was a small effect, however, which did not result in a significant change in the integrated cAMP response (**Figure 5D**). A similar but more pronounced effect was observed in the second KCTD12 KO clone, resulting in a significant increase of the integrated isoproterenol-induced cAMP response (**Figure S9C**). KCTD12 KO also appeared to enhance $G_i\alpha$-mediated inhibition of the cAMP response through endogenous SST receptors, and this effect was significant in both KO clones while varying in degree between them (**Figure 5E** and **Figure S9D**). We did not observe a comparable effect when $G_i\alpha$-mediated inhibition was elicited through overexpressed MOR (**Figure S9E**) but were able to elicit the converse effect, reduced MOR-mediated inhibition, when KCTD12 was overexpressed together with MOR and utilizing concentration-response analysis to assess signaling (**Figure S9F**). Previous studies indicate that

KCTD12 regulates signaling primarily through interactions with Gβγ subcomplexes, whereas cAMP production in HEK293 cells is regulated both by Gα and Gβγ subunits. Thus we considered that cAMP assay may not be an ideal readout of KCTD12 effects. Accordingly, we tested regulation of overexpressed GIRK channels as a more direct readout of signaling via Gβγ. Using DAMGO to elicit Gβγ release through MOR, we verified a rapid inward current followed by a slow 20-40% desensitization over the course of 60 seconds. KCTD12 KO did not detectably affect the initial current amplitude (**Figure S9G**) elicited by DAMGO but it impaired either the speed (**Figure 5F**) or extent of desensitization (**Figure S9H**), depending on the agonist dose applied. Conversely, overexpression of KCTD12 accelerated GIRK current desensitization (**Figure S9I**).

Together, these results indicate that both EYA4 and KCTD12 indeed impact cellular G protein responses, but their effects differ: EYA4 enhances the acute G_sα-mediated cAMP elevation, apparently by suppressing basal inhibition through G_iα, whereas KCTD12 promotes signal desensitization after the peak and impacts both G_sα and G_iα signaling apparently through Gβγ.

Discussion

APEX-mediated proximity labeling combined with quantitative MS represents a method to assess and compare the effects of diverse ligands on GPCR activation in an unbiased and medium throughput fashion. Its application and the interpretation of GPCR-APEX datasets has been limited by (1) the data complexity resulting from receptor trafficking to multiple compartments and (2) the lack of computational approaches that can deconvolve proximity labeling data into their constituent parts – spatial bystanders and functional proximal interaction networks. Here, we introduce a computational framework that addresses this limitation by predicting ligand-dependent receptor trafficking and thus accounting for the location-dependent component in the proximity labeling data.

A prerequisite for the framework is the *a priori* selection of relevant spatial references and their parallel processing with the GPCR-APEX samples. These spatial references allow estimating the proximity labeling background proteome followed by calculation of ligand-dependent coefficients for each selected subcellular compartment. Notably, the coefficients do not provide an absolute measure of the receptor at a given subcellular location, but rather give an estimate of its relative distribution within the cell and how this distribution dynamically changes over a time course of activation. Nevertheless, we demonstrate that the coefficients provide the means to subtract the majority of location-specific trends from the GPCR-APEX datasets.

Applying this framework to the mu-opioid receptor and its activation with three chemically distinct ligands, we reveal a distinct ligand-dependent trafficking behavior, and after detrending the data for location-specific effects, we were able to enrich for functionally relevant proteins in the receptor interaction network. This is exemplified by interactors with well-characterized function in GPCR signaling and trafficking such as ARRB2 and members of the Retromer and WASH complexes. However, it needs to be pointed out that the process of data detrending based on spatial references is not without limitations. It is based on a simplified assumption that the GPCR-APEX construct and the spatial references result in similar protein labeling patterns at a given location.

Given that GPCRs can traffic to multiple compartments and potentially reside in different subcellular microdomains compared to the spatial references, the simple assumption might not hold true for all proteins in the dataset. Therefore, we emphasize that functional characterization should be conducted to corroborate any hypotheses derived from the proximal interaction networks.

As an aside, it is perhaps worth emphasizing the striking differences in trafficking induced by the three agonists. Whereas DAMGO provoked strong internalization and subsequent trafficking of the MOR, this was much reduced by morphine, and was essentially undetectable by PZM21. This latter compound emerged from a structure-based effort to develop agonists functionally selective for $G_i\alpha$ versus arrestin recruitment,[15] leading to a compound with strong analgesic effects with reduced respiratory depression and constipation effects that are otherwise characteristic of MOR agonists. Whereas the precise mechanistic bases of the apparent functional selectivity of PZM21 and other "biased" agonists[35] remains controversial,[36,37] the differential trafficking of the MOR when activated by PZM21 does support differentiation from agonists like DAMGO and even morphine. The proteomic-based characterization of trafficking and downstream protein engagement described here offers arguably a holistic way of investigating functional selectivity, one that may be applied to the development of other functionally selective molecules in GPCR signaling.

We discovered novel components in the proximal interaction network of MOR, EYA4 and KCTD12, which change upon activation with all ligands in a $G_i\alpha$ activity-dependent manner. For EYA4 we describe a novel role in modulating $G_i\alpha$ signaling that is consistent with EYA4 directly binding $G_i\alpha$ subunits, to a limited degree at basal level, as our AP-MS data show, which is enhanced upon addition of agonist. Based on these results, we propose a simple model in which endogenous EYA4 binding to $G_i\alpha$ subunits sets a 'threshold' for $G_i\alpha$ inhibition by effectively sequestering $G_i\alpha$ subunits when produced at low basal levels, but being saturated by the higher $G\alpha i$ levels produced in response to agonist activation (**Figure 6A**). KCTD12 has been well-characterized as auxiliary subunit for $GABA_B$ receptors regulating the rise time and duration of GIRKs by competitive binding to $G\beta\gamma$ subunits. Our study shows that KCTD12 can impact G protein-mediated signaling through $G\beta\gamma$ for other receptors, as previously suggested.[33] In contrast to $GABA_B$ receptors, however, our data shows that KCTD12 does not constitutively bind to the C-tail of MOR. Rather, KCTD12 appears to be directly recruited to the dissociated $G\beta\gamma$ subunit following receptor activation. One simple model is that KCTD12 sequesters $G\beta\gamma$ subcomplexes produced under agonist-induced conditions, thus depleting G protein heterotrimers available for reactivation after prolonged agonist exposure (**Figure 6B**). While other possibilities cannot be presently excluded, and we note recent evidence for an additional effect of KCTD12 on adenylyl cyclase activity,[38] this simple model is attractive because it is sufficient to explain KCTD12 affecting both cAMP and GIRK signaling, as well as enhancing desensitization without changing the acute agonist response. Given that EYA4 and KCTD12 interact with the dissociated G protein subunits rather than with the receptor itself, we conclude (1) that they might regulate G protein signaling beyond MOR and (2) that GPCR-APEX has the sensitivity to monitor a proximal interaction network beyond its direct and indirect interactor partners.

Our framework is applicable to any proximity labeling dataset trying to discriminate protein interactions and location, which meets a major need as proximity labeling becomes more widespread. We believe it is a particular powerful method to assess and compare ligand-specific effects on GPCR activation. To our knowledge, it is the first methodology that can simultaneously capture the multiple layers of receptor activation-location and interaction networks in an unbiased and medium throughput fashion. As such we envisage that its application will prove to be key in drug discovery efforts to characterize and prioritize novel receptor ligands for *in vivo* testing in a medium throughput manner, but also inform hypothesis-driven exploration of the molecular mechanisms of how chemically distinct ligands can evoke different cellular responses.

Acknowledgements

This work was supported by funding from the Defense Advanced Research Projects Agency (DARPA) under the Cooperative Agreements HR0011-19-2-0020 (to N.J.K., M.v.Z., and R.H.) and HR0011-20-2-0029 (to N.J.K. and R.H.). The views, opinions, and/or findings contained in this material are those of the authors and should not be interpreted as representing the official views or policies of the Department of Defense or the U.S. Government. This work further received funding from the NIH (P01HL146366 to N.J.K. and R.H.; 1U01MH115747 to N.J.K. and M.v.Z.; R35GM124731 to J.L: R01DA010711 and DA012864 to M.v.Z.) and an NSF Graduate Research Fellowship (to N.A). B.T.L. was a recipient of a K99/R00 (DA043607). E.B. is supported by an NIH/NRSA Postdoctoral Fellowship (F32CA260118). J.L. is also supported by the Rohr Family Research Scholar Award and the Irma T. Hirschl and Monique Weill-Caulier Award.
The work was carried out in the Thermo Fisher Scientific Mass Spectrometry Facility for Disease Target Discovery at the J. David Gladstone Institutes and the UCSF Center for Advanced Technology. We thank Kirsten Obernier for reading the manuscript and providing critical feedback and members of both the von Zastrow lab and Krogan lab for helpful advice and comments.

Author Contributions

B.T.L., B.J.P., M.v.Z., and R.H. conceived and directed the study with input from N.J.K. APEX proximity labeling: B.T.L. and Q.L. Development of data analysis workflow and APEX data analysis: B.J.P. Electrophysiology: N.A. and J.L. Construct cloning: B.T.L. and J.X. AP-MS experiments: J.X. with input from R.H. AP-MS data analysis: Z.Z.C.N. with input from R.H. Knockout cell line generation: J.X. with input from R.H. cAMP measurements: E.B. and B.T.L. with input from M.v.Z.

Competing Interest Statement

The Krogan Laboratory has received research support from Vir Biotechnology and F. Hoffmann-La Roche. Nevan Krogan has consulting agreements with the Icahn School of Medicine at Mount Sinai, New York, Maze Therapeutics and Interline Therapeutics. He is a shareholder in Tenaya Therapeutics, Maze Therapeutics and Interline Therapeutics, and a financially compensated Scientific Advisory Board Member for GEn1E Lifesciences, Inc.

Online Methods

Mammalian Cell Culture Conditions

HEK293 cells (CRL-1583, ATCC) were cultured in Dulbecco's modified Eagle's medium (DMEM, GIBCO or Fisher Scientific), supplemented with 10% fetal bovine serum (UCSF Cell Culture Facility) and maintained at 37°C in a 5% CO_2 humidified incubator. HEK293 cells stably expressing APEX2-tagged constructs were selected with 500 µg/mL G418 and maintained in 100 µg/mL G418. Transfections were performed using Lipofectamine 2000 (Invitrogen) or Lipofectamine 3000 (Invitrogen) for cDNA (2 uL of Lipofectamine per 1 µg of DNA). For transient DNA expression, cells were transfected 24 or 48 hr before experiments. For electrophysiology measurements, cells were seeded on poly-L-lysine-coated 18 mm coverslips. Transfections were performed using Lipofectamine 2000 (Invitrogen).

Flow cytometric analysis of receptor trafficking

Flow cytometric analysis of receptor surface immunofluorescence was used to determine agonist induced internalization and subsequent agonist-withdrawn surface recovery (recycling). HEK293 cells stably expressing FLAG-tagged MOR were left untreated as a control, incubated with 10 µM DAMGO for the noted time (0-30 min). To measure recycling, cells were incubated with 10 µM DAMGO for 30 min, washed, and then incubated for an additional 30 min with 10 µM naloxone. All cells were washed twice in ice-cold PBS to stop trafficking, and incubated at 4°C for 45 min with 2 µg/mL Alexa647 (Life Technologies)-conjugated M1 anti-FLAG (Sigma F-3040). Cells were washed once in PBS at 4°C, and then mechanically lifted in PBS for an additional 45 min at 4°C. Median fluorescence intensity of 10,000 cells per condition was measured using a FACSCalibur instrument (Becton Dickinson). Internalization was calculated as a fraction of the agonist treated condition divided by untreated. Recycling was calculated as a fraction of surface recovered receptor divided by the internalized receptor. At least four independent biological experiments were performed in triplicate for each condition.

Live cell cAMP accumulation assay

HEK293 cells stably expressing MOR or MOR-APEX2 were transiently transfected with the cAMP biosensor pGLO-20F (Promega). Prior to agonist stimulation, cells were incubated with 250 µg/mL luciferin for 45 min in DMEM without phenol red or serum. 10 µM DAMGO and 10 nM isoproterenol or 10 nM isoproterenol (reference condition) were added to each well, and placed at 37°C. Luminescence was recorded every 10 s with a CCD sensor for 20 min. Luminescence signal generated agonist stimulation was integrated across 1 minute of maximum average signal for the given condition, and normalized to the integrated signal from 1 minute of the control condition.

cADDis cAMP biosensor assay

Real-time cAMP dynamics were measured using the Green Up cADDis cAMP biosensor (Montana Molecular) according to the manufacturer's protocol. Briefly, HEK293 cell lines were lifted using TrypLE Express (Thermo Fisher) and resuspended in media supplemented with the appropriate volume of cADDis BacMam. Cells were plated into a 96-well plate (Corning #3340) at a concentration of 50,000 cells per well. After resting at room temperature for 30 minutes, plates were incubated under normal culture conditions overnight. Plates were washed twice with assay buffer (20 mM HEPES pH 7.4, 135 mM NaCl, 5 mM KCl, 0.4 mM $MgCl_2$, 1.8 mM $CaCl_2$, 5 mM d-

glucose) before a ten minute incubation in a plate reader (Synergy H4, BioTek) pre-warmed to 37°C. Fluorescence was detected using an excitation wavelength of 500 nm and an emission wavelength of 530 nm every 30 seconds. After a five minute baseline reading, vehicle or agonist(s) (100 nM isoproterenol, 10 μM DAMGO, and 1 μM SST) were added, and fluorescence was measured for 30 minutes. A baseline fluorescence (F_0) was calculated for each well by averaging its fluorescence over the five minute baseline reading, and the fluorescence response at each timepoint was calculated as the change in fluorescence ($\Delta F = F - F_0$) normalized to the baseline (F_0). To calculate an integrated cAMP, data points after agonist addition were summed. Each biological replicate represents the average of at least two technical replicates.

APEX reaction, biotinylated protein enrichment and preparation for mass spectrometry analysis

For the MOR-APEX experiments the following method was used to perform biotinylation, enrichment and prepare the samples for MS analysis. 500 μM biotin-phenol was pre-incubated with cells expressing MOR-APEX2 for 30 min at 37°C. 10 μM DAMGO ([D-Ala2, N-Me-Phe4, Gly5-ol]-Enkephalin acetate salt, Sigma-Aldrich), morphine (Morphine sulfate, Sigma-Aldrich), or PZM21 (synthesized by Enamine at 98% purity as tested by NMR and LC-MS) was added for the noted period of time. For the spatial references, cells expressing PM-APEX2, Endo-APEX2, and Lyso-APEX2 were incubated with 500 μM biotin-phenol for 30 min at 37°C, no agonists were added to these cells. Immediately prior to use, H_2O_2 was diluted to 2 mM final in room-temperature media (DMEM+10% FBS). APEX labeling was initiated by 1:1 mixing of the H_2O_2 containing media (1 mM H_2O_2 final) with the biotin-phenol containing media at room temperature. The labeling reaction was allowed to continue for 30 s, media was removed, and the cells were washed three times in ice cold quenching buffer (TBS supplemented with 1 mM CaCl2, 10 mM sodium ascorbate, 1 mM sodium azide, and 1 mM Trolox). Cells were incubated in quenching buffer for 20 min on ice, quenching buffer was removed, and cells were lysed in RIPA (50 mM Tris, 150 mM NaCl, 1% Triton X-100, 0.5% deoxycholate, 0.1% SDS, pH 7.4) supplemented with 10 mM sodium ascorbate and protease inhibitors (Roche Complete). Samples were briefly sonicated, spun down at 10,000 x g for 10 min, the supernatant was applied to streptavidin agarose resin (Thermo), and incubated overnight at 4°C.

Streptavidin agarose resin was washed two times in RIPA buffer (50 bed volumes per wash), four times in TBS (50 bed volumes per wash), one time in 50 mM NH_4HCO_3, 3 M Urea (1 bed volume per wash). Samples were reduced on resin by adding TCEP (5 mM final) and incubating, with orbital shaking, for 30 min at 55°C. Samples were alkylated by adding iodoacetamide (10 mM final), covered from light and with orbital shaking, for 20 min at room temperature. The reaction was quenched upon addition of DTT (20 mM final). The streptavidin agarose resin was spun down and the buffer exchanged to 50 mM NH_4HCO_3, 2 M Urea. Biotinylated proteins were cleaved on resin by the incubation of trypsin overnight at 37°C (1 μg trypsin per 20 uL of streptavidin agarose). Following proteolysis, the resin was spun down by centrifugation at 1000 x g for 1 min, and supernatant collected. The resins were washed twice with 50 mM NH_4HCO_3, 2 M Urea and this material was pooled with the first supernatant. The sample was acidified with TFA. NEST C18 MacroSpin columns were used to desalt the peptide sample for mass spectrometric analysis.

For the PM-APEX and EYA4-APEX samples the following method was used to perform biotinylation, enrichment and prepare the samples for MS analysis. HEK293 cells expressing

MOR and either the PM-APEX or EYA4-APEX construct were incubated with 500 μM biotin-phenol at 37°C for 30 min. 10 μM DAMGO was added for 3 different time points including 1, 5, and 10 min for PM-APEX, and 10 min for EYA4-APEX. For the pertussis toxin treatment condition, cells were preincubated with 100 ng/ml pertussis toxin for 18 hr before DAMGO treatment. APEX labeling was initiated by 1:1 mixing of the H_2O_2 containing media (1 mM H_2O_2 final) with the biotin-phenol containing media at room temperature. After 45 s of the biotinylation reaction, the cells were washed three times (1 min each) with ice cold quenching buffer (PBS supplemented with 10 mM sodium ascorbate, 10 mM sodium azide, and 5 mM Trolox). Cells were then collected in 8 mL of quench buffer and pelleted by centrifugation at 4 °C for 10 min at 3000 g. For cell lysis, cells were homogenized using probe sonication in RIPA (50 mM Tris, 150 mM NaCl, 1% Triton X-100, 0.25% sodium deoxycholate, 0.25% SDS, pH 7.4) supplemented with 10 mM sodium ascorbate, 10 mM sodium azide, 5 mM Trolox, 1mM DTT, and protease inhibitors (Roche Complete). To remove the cell debris, cell lysate was centrifuged at 10,000 x g for 10 min, and the supernatant was taken for streptavidin enrichment of biotinylated proteins.

The enrichment of biotinylated proteins was automated with the KingFisher Flex (Thermo Fisher Scientific). Supernatants were incubated at 4 °C for 18 hrs with magnetic streptavidin beads (Pierce™ Streptavidin Magnetic Beads, Thermo Fisher Scientific) which were pre-washed twice with RIPA buffer. Following incubation, beads were washed three times with RIPA buffer, one time with 1 M KCl, one time with 0.1 M Na_2CO_3, one time with 2 M urea in 50 mM Tris-HCl (pH 8) buffer, and two times with 50 mM Tris-HCl (pH 8) buffer. Beads were maintained in 200 uL of 2 M urea in 50 mM Tris-HCl (pH 8) buffer for on-bead digestion of proteins. Samples were reduced with 5 mM TCEP at 37 °C for 30 min, followed by alkylation with 5 mM IAA at room temperature for another 30 min, which was quenched by addition of DTT (5 mM final). For tryptic digestion, 1 ug of trypsin was added to beads and incubated with shaking at 37 °C for 4 hrs. Supernatants were taken and saved for desalting using NEST C18 MicroSpin columns.

Unbiased mass spectrometric data acquisition and protein quantification for APEX samples

Digested peptide mixtures were analyzed by LC-MS/MS on a Thermo Scientific Orbitrap Fusion tribrid mass spectrometry system equipped with a Proxeon Easy nLC 1000 ultra high-pressure liquid chromatography and autosampler system. Samples were injected onto a C18 column (25 cm x 75 μm I.D. packed with ReproSil Pur C18 AQ 1.9 μm particles) in 0.1% formic acid and then separated with an 80 min gradient from 5% to 30% ACN in 0.1% formic acid at a flow rate of 300 nl/min. The mass spectrometer collected data in a data-dependent fashion, collecting one full scan in the Orbitrap at 120,000 resolution followed by collision-induced dissociation MS/MS scans in the dual linear ion trap with a maximum cycle time of 3 seconds between each full scan. Dynamic exclusion was enabled for 30 s with a repeat count of 1. Charge state screening was employed to reject analysis of singly charged species or species for which a charge could not be assigned.

The raw data were analyzed using the MaxQuant algorithm (version 1.5.5.1) for the identification and quantification of peptides and proteins.[39] Data were searched against the SwissProt Human database (downloaded 01/2017), augmented with the mouse Oprm and the APEX2 sequence, concatenated to a decoy database where each sequence was randomized in order to estimate the false discovery rate (FDR). Variable modifications were allowed for methionine oxidation and

protein N terminus acetylation. A fixed modification was indicated for cysteine carbamidomethylation. Full trypsin specificity was required. The first search was performed with a mass accuracy of ± 20 parts per million and the main search was performed with a mass accuracy of ± 4.5 parts per million. A maximum of 5 modifications and 2 missed cleavages were allowed per peptide. The maximum charge was set to 7+. Individual peptide mass tolerances were allowed. For MS/MS matching, the mass tolerance was set to 0.8 Da and the top 8 peaks per 100 Da were analyzed. MS/MS matching was allowed for higher charge states, water and ammonia loss events. The data were filtered to obtain a peptide, protein, and site-level false discovery rate of 0.01. The minimum peptide length was 7 amino acids. Results were matched between runs with a time window of 2 min for biological replicates. Peptide-ion intensities produced by MaxQuant from the spatial references together with the time-series MOR-APEX samples were summarized to protein intensities using the R package MSstats (version 3.23.1),[28] specifically the function *dataProcess* with default arguments except the outlier and noise filters[40] were enabled by setting "remove_uninformative_feature_outliers=TRUE" and "featureSubset='highQuality'". Log-transformed protein intensities were normalized per run using an equalize-medians procedure.

Digested PM-APEX and EYA4-APEX samples were analyzed on an Orbitrap Exploris 480 mass spectrometry system (Thermo Fisher Scientific) coupled to a Easy nLC 1200 nano-flow ultra high-pressure liquid chromatography (Thermo Fisher Scientific) interfaced via a Nanospray Flex nanoelectrospray source. Samples were reconstituted in 1% formic acid and loaded onto a C18 column (25 cm x 75 µm I.D. packed with ReproSil Pur C18 AQ 1.9 µm particles). Mobile phase A consisted of 0.1% FA, and mobile phase B consisted of 0.1% FA/80% ACN. Peptides were separated at a flow rate of 300 nl/min using a gradient increasing buffer B over 40 min to 16% B, followed by an increase over 26 min to 28% B and 4 min to 44% B. The mass spectrometer acquired data in a data-independent acquisition (DIA) mode, collecting one full scan in the Orbitrap at 120,000 resolution followed by DIA MS/MS scans within a m/z range of 350-1050 with a fragmentation window size set to 20 m/z. The resolution of orbitrap for MS2 scans was set to 15,000 and a normalized collision energy of 30 was used for fragmentation. The DIA data were analyzed with Spectronaut (Biognosys) using direct DIA analysis default parameters for the identification and quantification of proteins. Normalization in Spectronaut was turned off. Data were searched against the SwissProt Human database (downloaded 01/2017). Peptide ion intensities from Spectronaut were summarized to protein intensities using MSstats (version 3.22.1)[28] implemented in the R package artMS (version 1.8.3) with default settings.

Statistical analysis of unbiased MS data for APEX samples

MOR-APEX: Each protein's trend over the time course after treatment with agonists was scored by fitting the log2 intensities with continuous polynomial curves over time using the R functions *lm* and *poly*. To better fit the rapid changes, the collected timepoints were encoded by their ranks (1, 2, 3, 4, 5, and 6 for 0, 1, 5, 10, 30, and 60 minutes). All models included an additive term for the batch–a protein's background intensity was expected and allowed to vary between batches. Three time-dependent models were tested that varied in the maximum polynomial power that was allowed for the ranked-time model: linear, quadratic and cubic. The time-dependent models were compared with a null-model that contained only the batch term using the R function *anova* to

compute an F statistic and p-value. The time model with the lowest p-value was selected and the maximum model-predicted change between time 0 and a later time was used as the maximum log2 fold change for that protein. This process was repeated separately for the three agonists.
Spatial References: Proteins that varied between spatial references were scored with a single run of the MSstats function *groupComparison* to compare between each non-redundant pair of spatial references. The input to MSstats was the entire set of spatial references with the MOR-APEX data excluded. MSstats fits a single linear mixed model for each protein with a single categorical fixed-effect term for condition (spatial reference) and a random-effect term for batch. Using this model, MSstats reports pairwise differences in means as log2 fold change (log2FC), and a pairwise p-value calculated from a t-test assuming equal variance across all spatial references. A subset of 193 location-specific proteins was selected that could reliably distinguish locations by requiring p-value < 0.005 and log2FC > 1.0 and observed intensity in all three replicates of at least one spatial reference greater than the 50th percentile of all observed protein intensities.
Spatial coefficients and spatial detrending of MOR-APEX samples: For each MOR-APEX sample, coefficients were calculated to estimate the contribution of each spatial reference to the observed protein intensity. First, protein intensities were scaled linearly between 0 and 1 by setting the maximum observed intensity (across all spatial reference and MOR-APEX samples) for each protein to 1.0, and all other observations were set to the ratio of observed/maximum for that protein. Missing values were set to zero. A matrix representing protein intensities in the spatial references for all observed proteins, **F** (3 spatial reference columns by 4291 protein rows), was constructed using mean (per spatial reference) scaled intensity. The location specific subset matrix (**S**) was defined by using only the rows of **F** that match the 193 location-specific proteins defined in the previous section. Location coefficients for each MOR-APEX sample were then calculated using the non-negative least squares procedure in the R package nnls using the location-specific matrix **S** and the vector of location-specific protein scaled intensities from each MOR-APEX sample as inputs. We found this procedure would estimate low but non-zero coefficients where they were expected to be zero (e.g. for lysosome at 0 min) likely due to fitting noise in the MOR-APEX samples that the spatial references could not account for. To minimize these effects we used modified **S** matrices that included three additional randomized columns, by sampling from **S**. We repeated this randomization and nnls procedure 100 times and used the median value for the spatial reference coefficients. The three spatial reference coefficients for each MOR-APEX sample were then combined into a matrix **C** with 3 rows (spatial references) and 54 columns (MOR-APEX samples; 3 ligands x 6 timepoints x 3 replicates). Estimates for sample-specific location components of all protein intensities were then predicted as the matrix product of **F** X **C.** Location-detrended intensity values were then calculated by log-transforming both observed (logObserved) and predicted (logPredicted) intensity values and taking the difference, *logObserved - logPredicted*.

PM-APEX: Changes in biotinylation of proteins at the plasma membrane in response to DAMGO and/or PTX were analyzed by fitting log2 protein intensity data using linear models with the R function lm. The linear models included a term for time with DAMGO as a categorical variable, a term for +/- PTX, and also the interaction term: DAMGO x PTX which measures the significance of the different response to DAMGO with- versus without- PTX.

EYA4-APEX: Changes in biotinylation of proteins neighboring EYA4 in response to DAMGO and/or PTX were analyzed by the R package artMS (version 1.8.3) which makes use of the groupComparison function with default settings implemented in MSstats (version 3.22.1).[28]

GO Enrichment method

Sets of proteins with significant changes were tested for enrichment of Gene Ontology terms (GO Biological Process, Molecular Function and Cellular Component). The over-representation analysis (ORA) was performed using the enricher function from R package clusterProfiler (version 3.99.0).[41] The gene ontology terms and annotations were obtained from the R annotation package org.Hs.eg.db (version 3.12.0). In order to reduce the set of significantly enriched terms (at FDR < 0.01) to a set of non-redundant GO terms, we first constructed a term tree based on distances (1-Jaccard Similarity Coefficients of shared genes in GO) between all significant terms using the R function hclust. The term tree was cut at a specific level (R function cutree, h = 0.99) to identify clusters of non-redundant gene sets. For results with multiple significant terms belonging to the same cluster, we selected the most significant term (i.e., lowest adjusted p-value).

GSEA on changing locations of EYA4-APEX

Significant cellular location changes between conditions were measured using gene set enrichment analysis as implemented in the R package fgsea (v 1.17).[42] Changes in protein intensity were scored using log2 fold change comparing samples and without DAMGO. Proteins were assigned to locations according to their “NMF Localization” from Human Cell Map (Version 1) downloaded on June 7, 2021 (https://humancellmap.org/resources/downloads/preys-latest.txt). The function fgsea was used with default options, and the log10 p-value with its sign changed to match direction of enrichment was used as the significance score.

Targeted mass spectrometric data acquisition for APEX samples

SRM assays were generated for selected interactors of MOR as well as localization controls and ribosomal proteins as internal controls for normalization (**Table S6**). SRM assay generation was performed using Skyline.[43] For all targeted proteins, proteotypic peptides and optimal transitions for identification and quantification were selected based on a spectral library generated from the shotgun MS experiments. The Skyline spectral library was used to extract optimal coordinates for the SRM assays, e.g., peptide fragments and peptide retention times. For each protein 2-5 peptides were selected based on intensity, peptide length as well as chromatographic performance. For each peptide the 3-6 best SRM transitions were selected based on intensity and peak shape.

Digested peptide mixtures were analyzed by LC-SRM on a Thermo Scientific TSQ Quantiva MS system equipped with a Proxeon Easy nLC 1200 ultra high-pressure liquid chromatography and autosampler system. Samples were injected onto a C18 column (25 cm x 75 µm I.D. packed with ReproSil Pur C18 AQ 1.9 µm particles) in 0.1% formic acid and then separated with an 80 min gradient from 5% to 40% Buffer B (90% ACN/10% water/0.1% formic acid) at a flow rate of 300 nl/min. SRM acquisition was performed operating Q1 and Q3 at 0.7 unit mass resolution. For each peptide the best 4 transitions were monitored in a scheduled fashion with a retention time window of 4 min and a cycle time fixed to 2 s. Argon was used as the collision gas at a nominal pressure of 1.5 mTorr. Collision energies were calculated by, CE = 0.0348 $*$ (m/z) + 0.4551 and

CE = 0.0271 ∗ (m/z) + 1.5910 (CE, collision energy and m/z, mass to charge ratio) for doubly and triply charged precursor ions, respectively. RF lens voltages were calculated by, RF = 0.1088 ∗ (m/z) + 21.029 and RF = 0.1157 ∗ (m/z) + 0.1157 (RF, RF lens voltage and m/z, mass to charge ratio) for doubly and triply charged precursor ions, respectively. The resulting data was analyzed with Skyline for identification and quantification of peptides.[43] MSstats (version 3.10.6) was used for statistical analysis.[28] Normalization across samples was conducted based on selected global standard proteins (RPL18A, RPL22, RPL28, RPL30, RPL35A, RPL6, RPL9, RPL9P7, RPL9P8, RPL9P9, RPS11). Model-based sample quantification implemented in MSstats was used to calculate the intensity of each protein in each biological sample and replicate combining all SRM transition intensities.

Shotgun proteomics data access

RAW data and database search results have been deposited to the ProteomeXchange Consortium via the PRIDE partner repository[44] with the dataset identifier PXD031415.

Targeted proteomics data access

Raw data and SRM transition files can be accessed, queried, and downloaded via Panorama[45] https://panoramaweb.org/MOR-APEX.url.

EYA4 affinity purifications

For each affinity purification (EYA4 wt, EYA4 A633R mutant, EYA4 D375N, one GFP control, one empty vector control), HEK293 cells stably expressing MOR were plated per 15-cm dish and transfected with 10 µg of individual Strep-tagged expression constructs (2 µg for Gfp) after 20–24 hours. Total plasmid was normalized to 15 µg with empty vector and complexed with PolyJet Transfection Reagent (SignaGen Laboratories) at a 1:3 µg:µl ratio of plasmid to transfection reagent based on manufacturer's recommendations. After more than 38 hours, cells were dissociated at room temperature using Dulbecco's Phosphate Buffered Saline without calcium and magnesium (D-PBS) supplemented with 10 mM EDTA and subsequently washed with D-PBS. Each step was followed by centrifugation at 200 × g, 4°C for 5 minutes. Cell pellets were frozen on dry ice and stored at −80°C. For each bait and control, n=3 independent biological replicates were prepared for affinity purification.

Frozen cell pellets were thawed on ice and suspended in 1 ml Lysis Buffer [IP Buffer (50 mM Tris-HCl, pH 7.4 at 4°C, 150 mM NaCl, 1 mM EDTA) supplemented with 0.5% Nonidet P 40 Substitute (NP40; Fluka Analytical) and cOmplete mini EDTA-free protease and PhosSTOP phosphatase inhibitor cocktails (Roche)]. Samples were subjected to freeze-thaw cycle before incubation on a tube rotator for 30 minutes at 4°C and centrifugation at 13,000 × g, 4°C for 15 minutes to pellet debris. Affinity purifications were performed as follows. MagStrep "type3" beads (30 µl per sample; IBA Lifesciences) were equilibrated twice with Wash Buffer (IP Buffer supplemented with 0.05% NP40) and incubated with the lysate on a tube rotator for 2 hours at 4°C. Following incubation, beads were washed twice with Wash Buffer and with IP Buffer. To directly digest bead-bound proteins, beads were resuspended in Denaturation-Reduction Buffer (2 M urea, 50 mM Tris-HCl pH 8.0, 1 mM DTT). Bead-bound proteins were denatured and reduced at 37°C for 30 min and after bringing them to room temperature, alkylated in the dark with 3 mM iodoacetamide for 45 min and quenched with 3 mM DTT for 10 min. Proteins were then incubated at 37°C, initially for

4 hours with 1.5 µl trypsin (0.5 µg/µl; Promega) and then another 1–2 hours with 0.5 µl additional trypsin. All steps were performed with constant shaking at 1,100 rpm on a ThermoMixer C incubator. Resulting peptides were combined with 50 µl 50 mM Tris-HCl, pH 8.0 used to rinse beads and acidified with trifluoroacetic acid (0.5% final, pH < 2.0). Acidified peptides were desalted for MS analysis using a BioPureSPE Mini 96-Well Plate (20mg PROTO 300 C18; The Nest Group, Inc.) according to standard protocols.

Samples were resuspended in 4% formic acid/2% acetonitrile solution and analyzed on an Q-Exactive Plus MS system (Thermo Fisher Scientific) equipped with an Easy nLC 1200 ultra-high pressure liquid chromatography system (Thermo Fisher Scientific) interfaced via a Nanospray Flex nanoelectrospray source. Samples were loaded onto a 75 µm ID C18 reverse phase column packed with 25 cm ReprosilPur 1.9 µm, 120Å particles (Dr. Maisch). Mobile phase A consisted of 0.1% FA, and mobile phase B consisted of 0.1% FA/80% ACN. Peptides were separated by an organic gradient ranging from 4.5% to 32% acetonitrile over 53 minutes, then held at 90% B for 9 minutes at a flow rate of 300 nl/min delivered by an Easy1200 nLC system (Thermo Fisher Scientific). All MS1 spectra were collected with orbitrap detection at a 70,000 resolution and a scan range from 300 to 1,500 m/z, while the 20 most abundant ions were fragmented by HCD and detected at a resolution of 17,500 in the orbitrap. All AP-MS data was searched against the SwissProt Human (downloaded 01/2017) using the default settings for MaxQuant (version 1.6.3.3).[39] Detected peptides and proteins were filtered to 1% false discovery rate in MaxQuant, and identified proteins were then subjected to protein-protein interaction scoring with both SAINTexpress (version 3.6.3)[46] and CompPASS.[47] We applied a filtering strategy to determine the final list of reported interactors. All protein interactions that possess a CompPASS WD score percentile > 0.95, a SAINTexpress BFDR ≤ 0.05. CompPASS scoring was performed using a larger in-house database derived from 11 baits that were prepared and processed in an analogous manner to this AP-MS dataset. This was done to provide a more comprehensive collection of baits for comparison, to minimize the classification of non-specifically binding background proteins as high confidence interactors. To determine the mutant-dependent changes in protein interactions of EYA4, protein abundances for mutant and wildtype AP-MS were compared using MSstats (version 3.14.1).[28] Protein interaction network was visualized using Cytoscape (version 3.8.1).[48]

Electrophysiology

Whole cell patch clamp experiments were performed as previously described.[49] Briefly, HEK 293 µOR stable cells were transfected with 0.7 µg GIRK1-F137S[50] and 0.1 µg tdTomato (tdT), per well. HEK 293T cells were transfected with GIRK1-F137S, 0.1 µg tdT, 0.35 µg µOR, with or without 0.7 µg GFP-KCTD12, per well. Experiments were performed at least 24 hr after transfection in a high potassium extracellular solution composed of (in mM) 120 KCl, 25 NaCl, 10 HEPES, 2 $CaCl_2$, and 1 $MgCl_2$ (pH 7.4). Solutions were delivered to a recording chamber using a gravity-driven perfusion system with exchange times of ~1 s. Cells were voltage-clamped at −60 mV using an Axopatch 200B amplifier (Molecular Devices). Patch pipettes with resistances of 3-7 MΩ were filled with an intracellular solution composed of (in mM): 140 KCl, 10 HEPES, 3 Na_2ATP, 0.2 Na_2GTP, 5 EGTA, 3 $MgCl_2$ (pH 7.4). Inward GIRK currents were induced with perfusion of 100 nM or 10 µM DAMGO. Desensitization of currents was measured over 60 s DAMGO application. Recordings were analyzed using Clampfit (Molecular Devices) and Prism

(GraphPad). Desensitization of the DAMGO-induced currents was calculated as follows: 100 ∗ (1 – (amplitude prior to DAMGO washout) / (peak amplitude following DAMGO application)). The tau of desensitization was calculated from the peak amplitude to DAMGO washout, fit to a single exponential curve.

Generation and characterization of CRISPR knockout cell lines for KCTD12 and EYA4

KCTD12 and EYA4 knockout (KO) cells lines were generated by electroporation of Cas9 ribonucleoprotein complexes (Cas9 RNPs) into HEK293 cells stably expressing MOR followed by clonal selection and characterization of the KO. Electroporation was performed using the SF Cell Line 4D-Nucleofector X Kit S (Lonza) and 4D-Nucleofecter (Lonza). Recombinant S. pyogenes Cas9 protein used in this study contains two nuclear localization signal (NLS) peptides that facilitate transport across the nuclear membrane. The protein was obtained from the QB3 Macrolab, University of California, Berkeley. Purified Cas9 protein was stored in 20 mM HEPES at pH 7.5 plus 150mM potassium chloride, 10% glycerol, and 1mM tris(2-carboxyethyl)phosphine (TCEP) at −80°C. crRNAs targeting EYA4 (5′-CCGTAAGTGGGCAAGCTGTA-3′) and KCTD12 (5′-CGTGACCCGGCGCTGCACGG-3′) were designed by Dharmacon. Each crRNA and the tracrRNA was chemically synthesized (Dharmacon) and suspended in 10 mM Tris-HCl pH 7.4 to generate 160 µM RNA stocks. To prepare Cas9 RNPs, crRNA and tracrRNA were first mixed 1:1 and incubated 30 min at 37°C to generate 80 µM crRNA:tracrRNA duplexes. An equal volume of 40 µM S. pyogenes Cas9-NLS was slowly added to the crRNA:tracrRNA and incubated for 15 min at 37°C to generate 20 µM Cas9 RNPs. For each reaction, roughly $3x10^5$ HEK293 cells were pelleted and suspended in 20 µL nucleofection buffer. 4 µL 20 µM Cas9 RNP mix was added directly to these cells and the entire volume transferred to the bottom of the reaction cuvette. Cells were electroporated using program CM-130 on the Amaxa 4D-Nucleofector (Lonza). 80 µL pre-warmed complete DMEM was added to each well and the cells were allowed to recover for 5 min at 37°C followed by dilution in complete DMEM media for limited dilution to generate clonal cell lines. Clonal cell lines were characterized by genomic sequencing to confirm gene editing of EYA4 and Western Blot analysis for KCTD12 (Cell Signaling, Cat# 81935S) to assess reduction in protein expression.

Figures

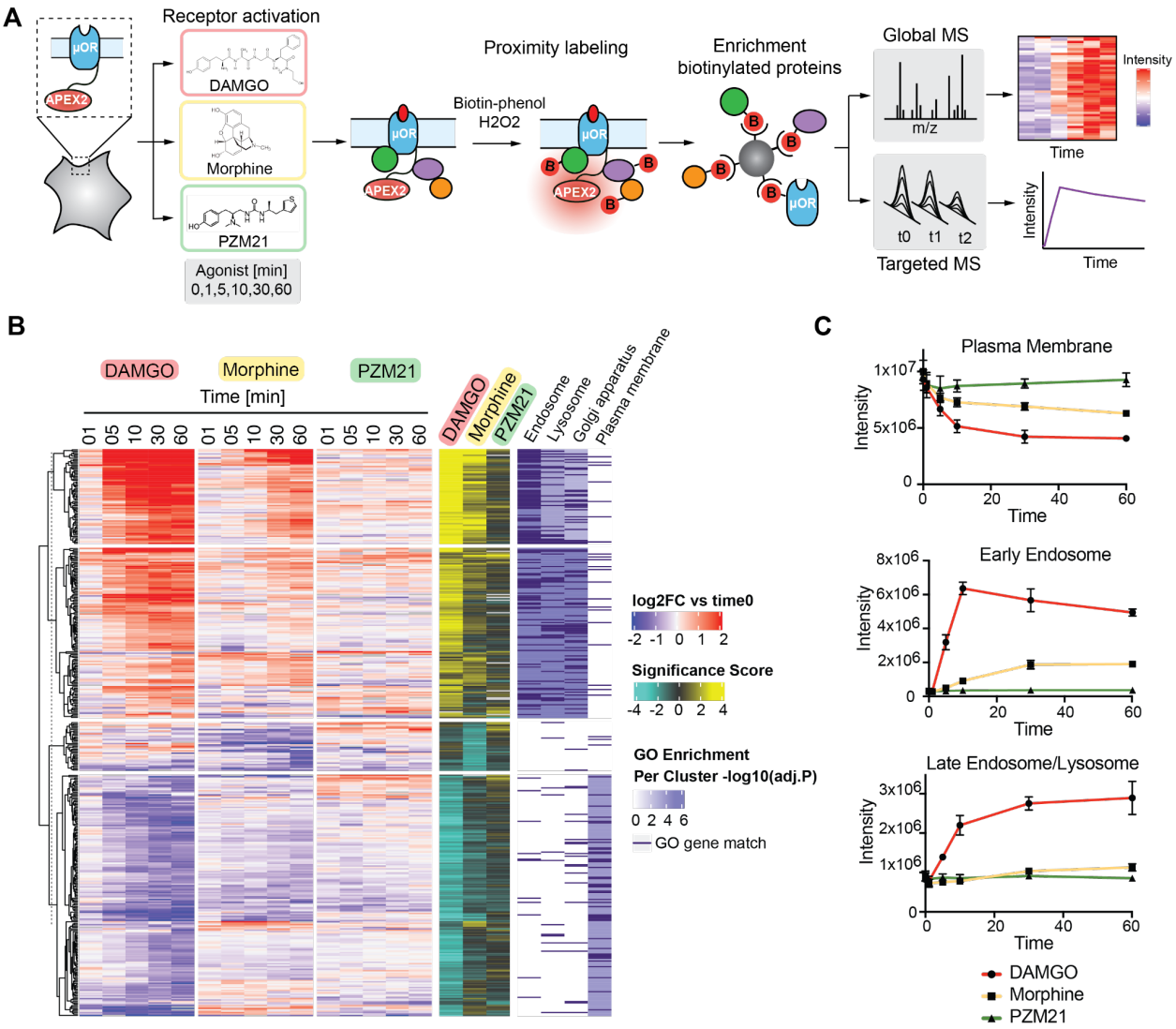

Figure 1. Ligand-dependent proximal proteome changes of the mu-opioid receptor are driven by cellular location.

A. Experimental design of the study. MOR-APEX constructs were stably expressed in HEK cells. The receptor was activated with 10μM DAMGO, morphine and PXM21 over a time course of 60 min. Cells were pretreated with biotinphenol for 30min and biotinylation was initiated by the addition of H_2O_2 for 30 sec at indicated time points after agonist treatment. Following cell lysis, biotinylated proteins were enriched using streptavidin and subsequently quantified using global and targeted mass spectrometry approaches.

B. Global agonist-dependent changes in proximal proteome of MOR. Heatmap visualizing all proteins with a significant ($p < 0.01$, $\log_2$ fold change > 1) change in biotin labeling for at least one of the ligands across the time course. The heatmap was clustered according to the significance score, calculated as a combination of the $-\log_{10}$ p-value and $\log_2$ fold change. Gene ontology enrichment analysis was performed for the individual clusters and

significant gene ontology terms for the individual clusters as well as the matching genes are indicated in dark purple. Data from three independent experiments are presented as mean.

C. Targeted proteomics analysis of agonist-dependent biotinylation by MOR-APEX2 of selected localization markers for plasma membrane (top), early endosome (middle), and late endosome/lysosome (bottom). Data from 3 different replicates for DAMGO (red), morphine (yellow), and PZM21 (green) are presented as mean + SEM.

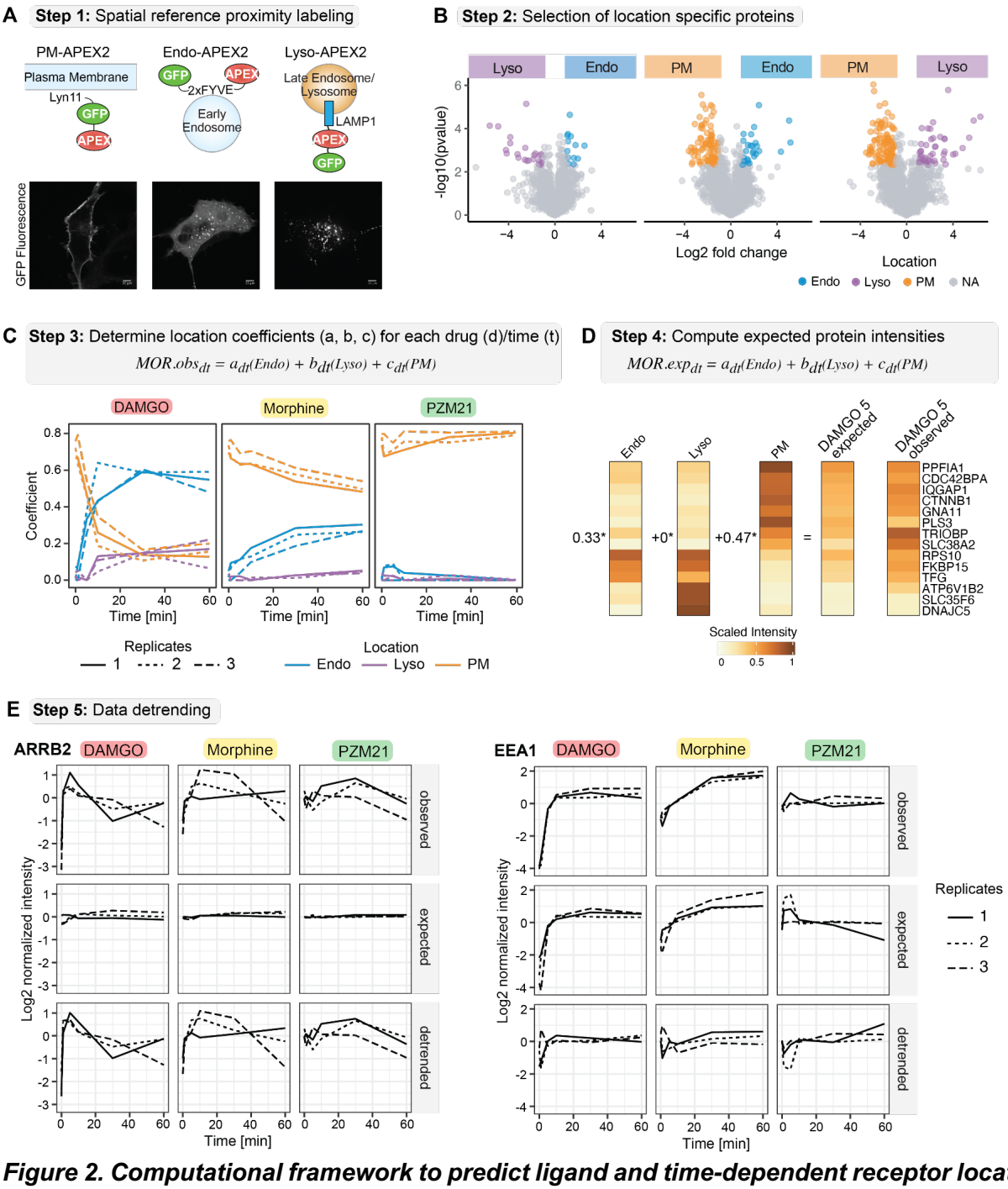

Figure 2. Computational framework to predict ligand and time-dependent receptor location and deconvoluting receptor location from local interaction network.

A. Step 1: Proximity labeling of spatial references. APEX-tagged constructs targeting APEX2 to the plasma membrane (PM-APEX2), early endosome (Endo-APEX2), or Lysosome (Lyso-APEX2) (top). Micrographs of PM-APEX2, Endo-APEX2, and Cyto-APEX2 using live-cell confocal imaging (scale bar, 10 μm) (bottom).

B. Step 2: Selection of location specific indicator proteins. Volcano plots depicting pairwise comparison of spatial references. Proteins with (1) a p-value below 0.005 and a fold change higher than 1.0 for at least one of the comparisons and (2) were required to be

consistently quantified across all replicates with an intensity greater than the 50th percentile were selected as location specific proteins for plasma membrane (PM, organe), Endosome (Endo, blue), and Lysosome (Lyso, purple). Data from three independent experiments are presented as mean.

C. Step 3: Determination of location specific coefficients. Intensities of location specific indicators proteins are utilized to calculate coefficients for each location and ligand based on the linear model. Data from three independent experiments are presented.
D. Step 4: Computing expected protein intensities. Expected intensities for all proteins quantified in the dataset are calculated based on location specific coefficients and protein intensities measured for the spatial references. A subset of the data is shown as an example.
E. Step 5: Data detrending. Data detrending process to dissect localization specific effect from effect of interaction with the receptor is exemplified for ARRB2 (known MOR interactor) and EEA1 (location specific protein). Three different temporal profiles are depicted for each protein, ligand, and replicate: the initial observed intensities, the expected intensities based on the location specific references, and the intensities after detrending. Data from three independent experiments are presented.

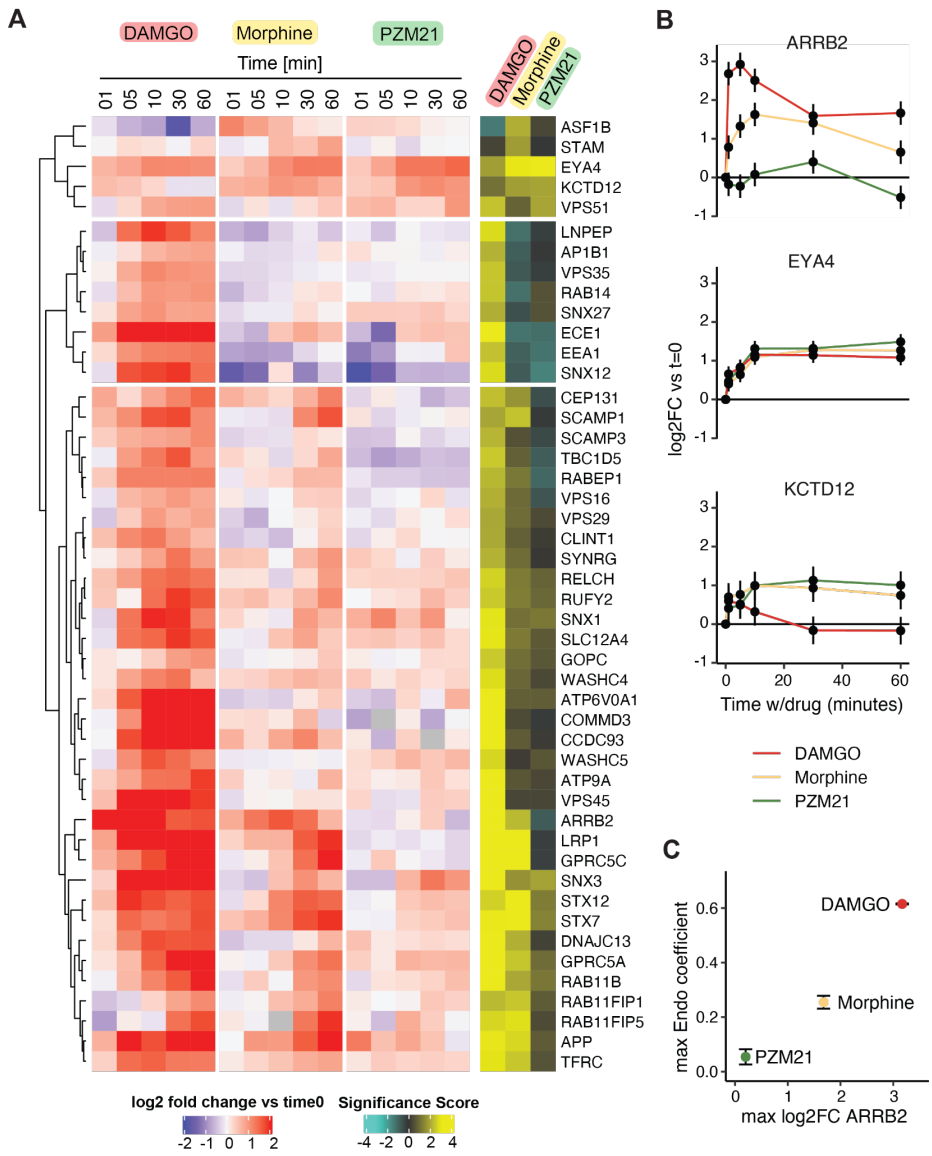

Figure 3. Ligand-dependent local interaction networks of MOR.

A. Ligand-dependent proximal protein interaction networks of MOR. All proteins are visualized in the heatmap that showed a significant difference in biotin labeling (log2FC > 1 and p-value < 0.001) before and after location-specific detrending for at least one of the ligands across the time course. The heatmap was clustered according to the significance score calculated as a combination of the $-\log_{10}$ p-value and $\log_2$ fold change. Data from three independent experiments are presented as mean.

B. Temporal profile for selected proteins in the MOR proximal interaction network. Line charts represent the $\log_2$ fold change over the time course of receptor activation with DAMGO (red), morphine (yellow) and PZM21 (green) after data detrending. Data from three independent replicates are presented as mean ± SEM.

C. Correlation between the maximum location coefficient calculated for the Endosome (Endo) and the maximum ARRB2 log2FC over the time course of MOR activation with DAMGO (red), morphine (yellow) and PZM21 (green).

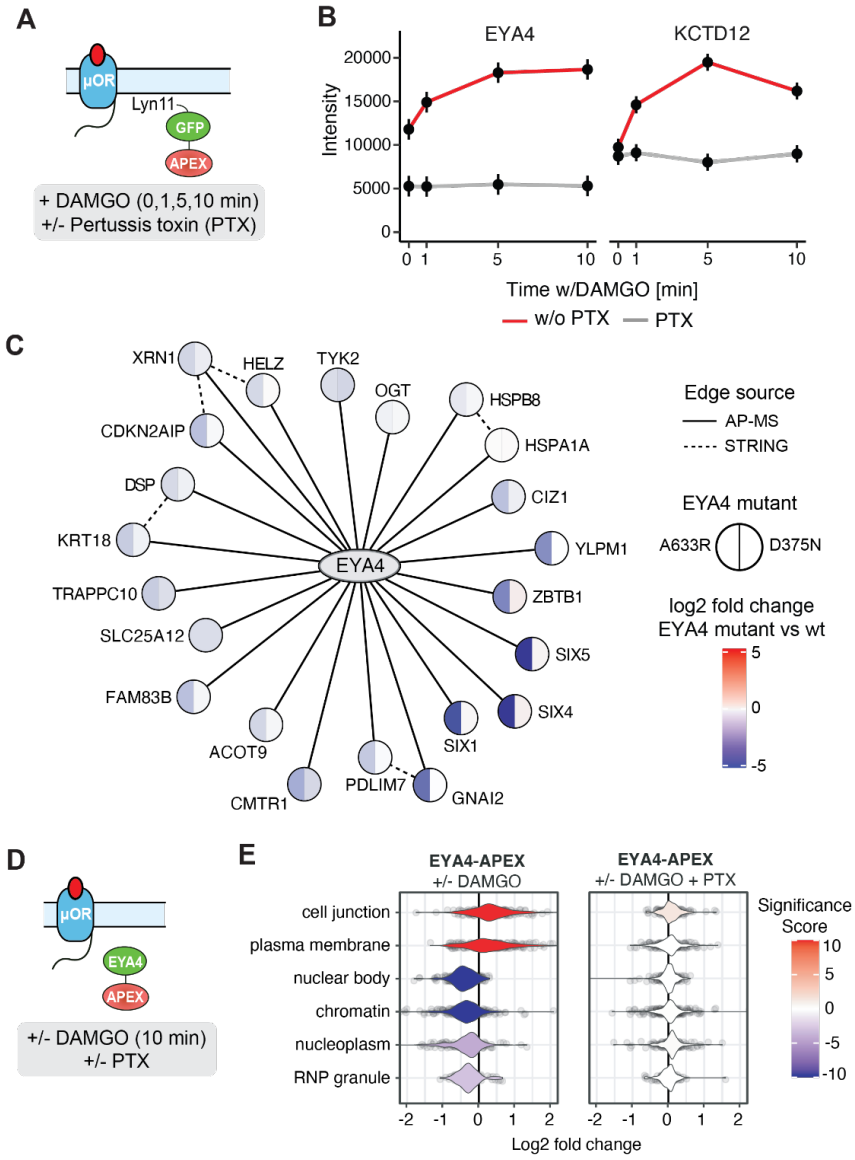

Figure 4. EYA4 and KCTD12 are recruited in the proximal interaction network of MOR in a Gαi activity-dependent manner.

A. APEX-based proximity labeling of the plasma membrane spatial reference construct (PM-APEX) was performed in a cell line expressing MOR in the presence and absence of the Gαi inhibitor Pertussis toxin (PTX) and after activation of MOR using DAMGO.

B. Line charts depict protein intensity for KCTD12 and EYA4 in PM-APEX experiment determined by quantitative MS over the DAMGO time course in the presence (grey) and absence of PTX (red). Data from three independent replicates are presented as mean ± SEM.

C. Interaction network of high-confidence interactors of EYA4 determined by affinity purification. Split nodes indicate protein abundance differences for the high-confidence interactors upon introduction of SIX-binding mutant (A633R) and phosphatase-dead mutant (D375N). Data from three independent replicates are presented as mean.

D. APEX-based proximity labeling of EYA4 was performed in a cell line expressing MOR in the presence and absence of the Gαi inhibitor Pertussis toxin (PTX) and after activation of MOR using DAMGO. Volcano plot depicting log10 p-value and log2 fold change comparing biotin labeled proteins in the proximity of EYA4 in the presence and absence of MOR activation by treatment with 10 μm DAMGO for 10 min. Data from three independent replicates are presented as mean.
E. Gene set enrichment analysis (GSEA) in log2FC depicted in **Figure S7** using the location-specific sets of proteins defined in Human Cell Map.

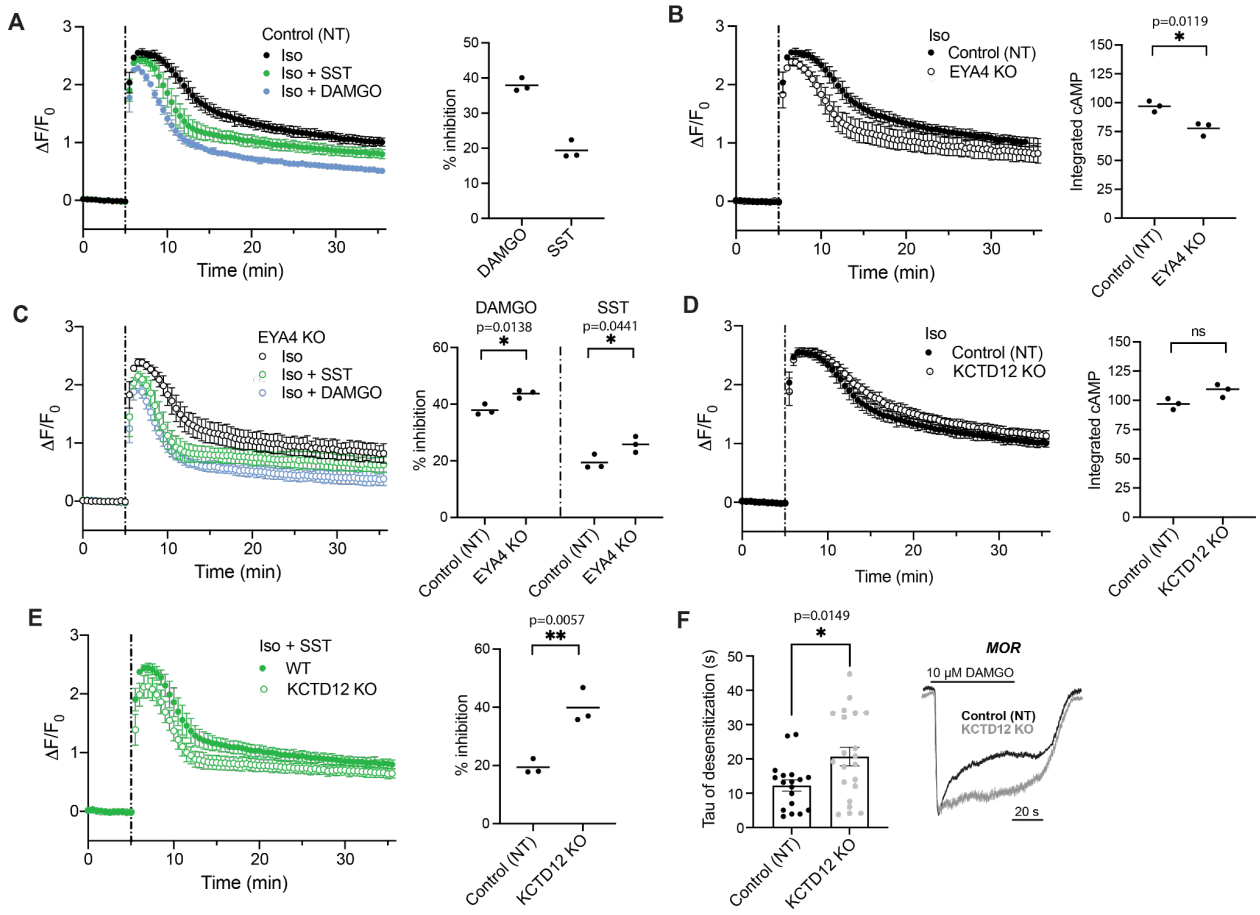

Figure 5. EYA4 and KCTD12 modulate G protein mediated signaling.

A. cAMP activity in HEK293 control non-targeting (NT) cells stably expressing MOR. Change in fluorescence intensity of cAMP biosensor upon stimulation with 100 nM isoproterenol (Iso) without (black) and with co-application of 1 μM somatostatin (SST, green) or 10 μM DAMGO (blue) is plotted.

B. cAMP activity in control (closed) and EYA4 KO (open) cells upon stimulation with Iso. Control curve repeated from panel A.

C. cAMP activity in EYA4 KO cells upon stimulation with Iso, with and without co-application of SST or DAMGO. Percent inhibition for Control (NT) repeated from panel A. Iso curve repeated from B.

D. cAMP activity in control (closed) and KCTD12 KO (open) HEK293 cells stably expressing MOR upon stimulation with Iso. Control curve repeated from panel A.

E. cAMP activity in control and KCTD12 KO cells upon stimulation with Iso and SST. Percent inhibition for control repeated from panel A. For all cAMP panels, N ≥ 3 and error bars represent standard deviation.

F. Left, Quantification of the tau of desensitization of MOR-mediated GIRK currents over 60 s 10 μM DAMGO application, in control and KCTD12 KO HEK cells. Each point represents an individual cell. Unpaired t-test, *p=0.0149. Error bars represent SEM. Right, representative whole cell patch clamp recording displaying GIRK currents mediated by MOR activation over 60 s DAMGO, in control and KCTD12 KO cells.

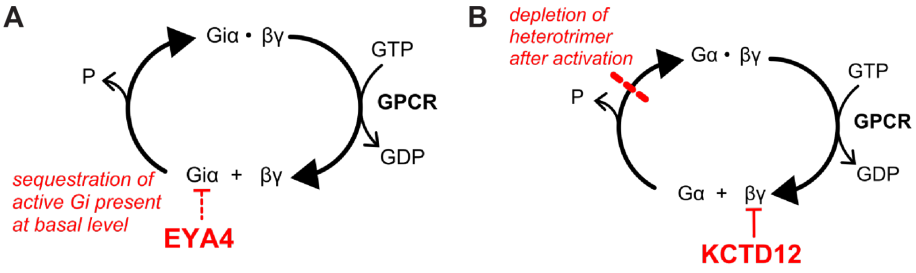

Figure 6. Possible models for distinct effects of EYA4 and KCTD12 on G protein mediated signaling. Model of EYA4 (A) and KCTD12 (B) effects on G protein signaling.

Supplemental Figures

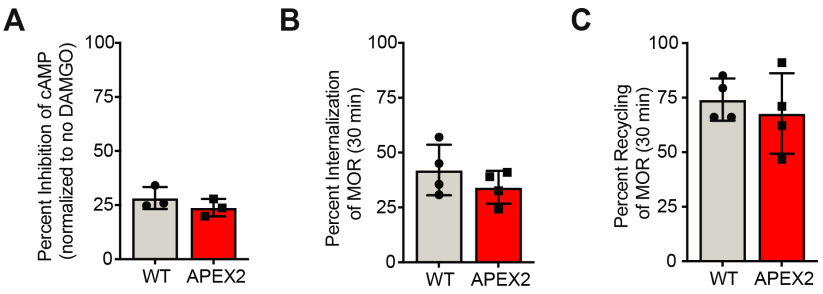

Figure S1. APEX-tagged MOR remains functional in signaling, internalization and recycling.

A. Receptor signaling was measured using a commercial cAMP biosensor (pGloSensor-20F). cAMP accumulation was measured after ~10 minutes of DAMGO/isoproterenol incubation and normalized to isoproterenol alone. Data from three independent experiments are presented as mean ± SEM.

B. Comparison of agonist-stimulated receptor internalization as assayed by loss of cell surface immunoreactivity and measured by flow cytometry comparing untreated (control) and treated samples (10 μM DAMGO, 30 min). Data from four independent experiments are presented as mean ± SEM.

C. Comparison of cell surface recovery of receptors ('recycling') following 30 min of DAMGO application (10 μM), agonist removal, and a 30 min recovery period in the presence of antagonist (10 μM). Data from four independent experiments are presented as mean ± SEM.

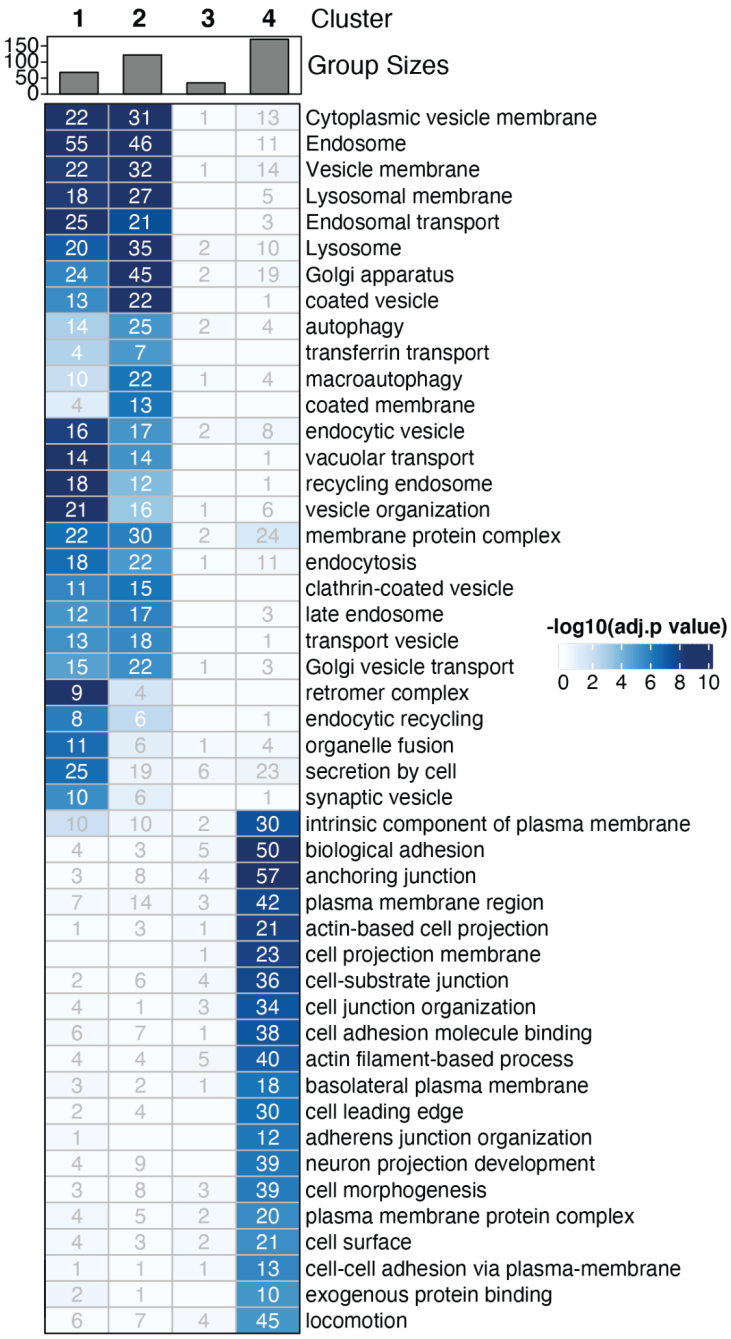

Figure S2. Gene ontology enrichment analysis for proteins of the ligand-dependent proximal interaction networks of MOR.

The heatmap shows all significantly enriched gene ontology terms (adjusted p-value < 0.05) among the proteins that significantly change in the proximal protein environment of MOR upon activation with DAMGO, morphine, or PZM21 including the number of proteins that match the gene ontology terms.

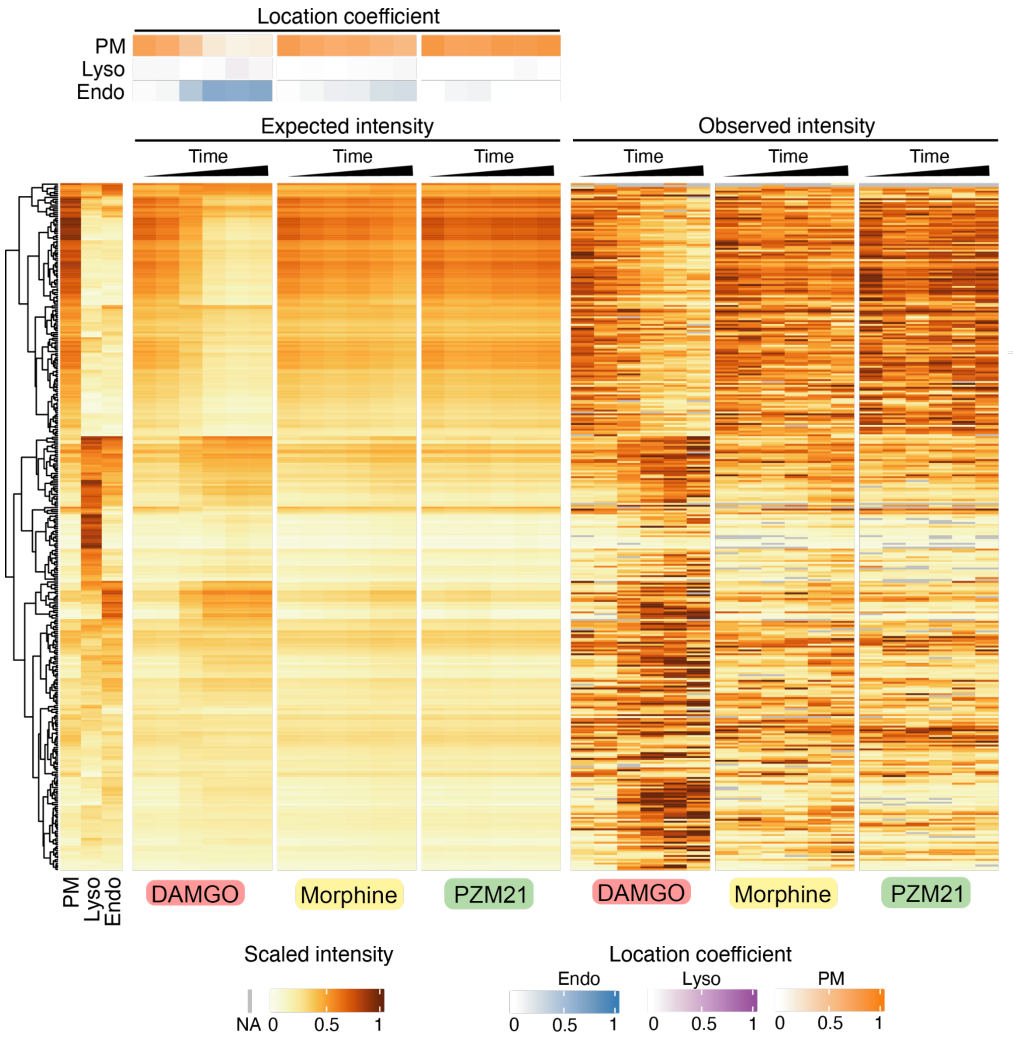

Figure S3. Prediction of expected protein intensities based on location coefficients.
The heatmap shows the location specific proteins that were selected by pairwise comparison of the spatial reference data and their scaled intensity measured across the spatial references (left side of the heatmap). Agonist and time point dependent expected protein intensities were estimated by summing the spatial reference protein intensities that were weighted with their respective location coefficient. Observed protein intensities are shown as comparison (right side of the heatmap). Data from three independent experiments are presented as mean.

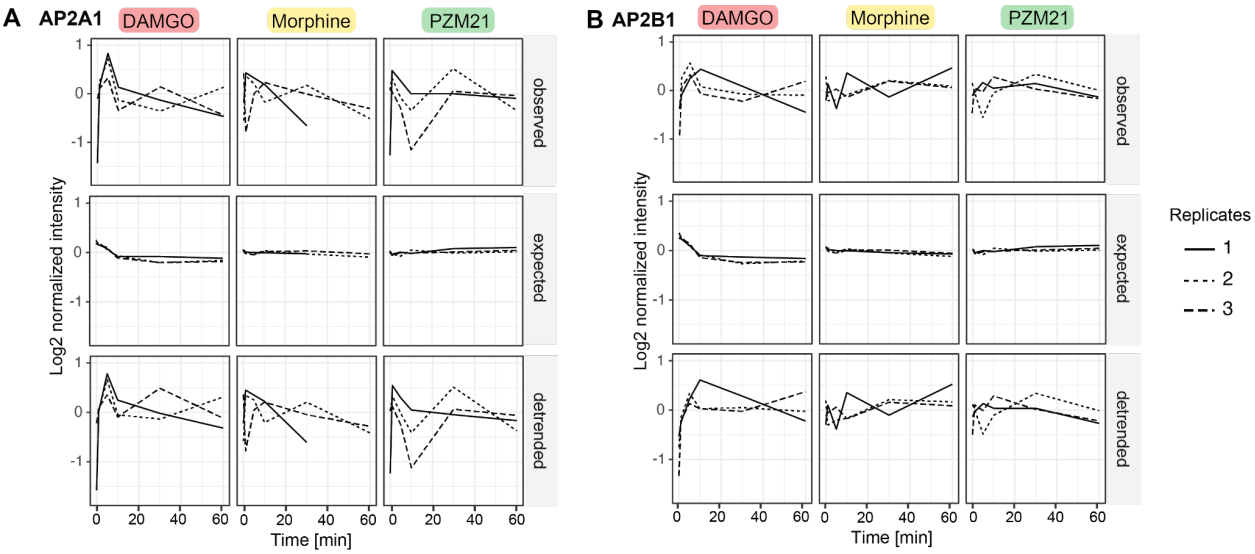

Figure S4. Effect of data detrending for AP2 complex subunits.

Data detrending process to dissect localization specific effect from effect of interaction with the receptor for AP2B1 and AP2A1, members of the adaptor protein complex. Three different temporal profiles are depicted for each protein, ligand, and replicate: the initial observed intensities, the expected intensities based on the location specific references, and the intensities after detrending. Data from three independent experiments are presented.

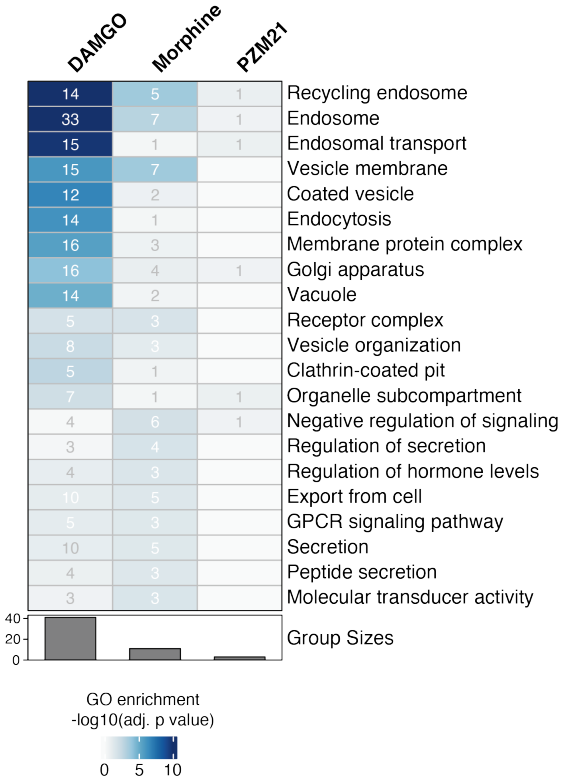

Figure S5. Gene ontology enrichment analysis for proteins of the ligand-dependent proximal interaction networks of MOR.

The heatmap shows all significantly enriched gene ontology terms (adjusted p-value < 0.05) among the proteins present in the proximal interaction network of MOR including the number of proteins that match the gene ontology terms.

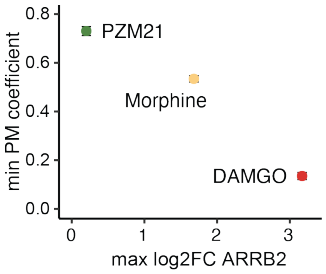

Figure S6. Correlation between ARRB2 engagement upon MOR activation with receptor trafficking.

Correlation between the minimum location coefficient calculated for the plasma membrane (PM) and the maximum ARRB2 log2FC over the time course of MOR activation with DAMGO (red), morphine (yellow) and PZM21 (green).

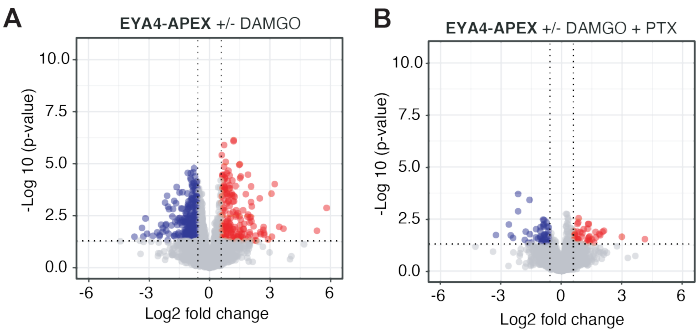

Figure S7. Changes in proximity labeling of EYA4 upon MOR activation.

Volcano plot depicting log10 p-value and log2 fold change comparing biotin labeled proteins in the proximity of EYA4 in the presence and absence of MOR activation by treatment with 10 μm DAMGO for 10 min and treatment with PTX. Data from three independent replicates are presented as mean.

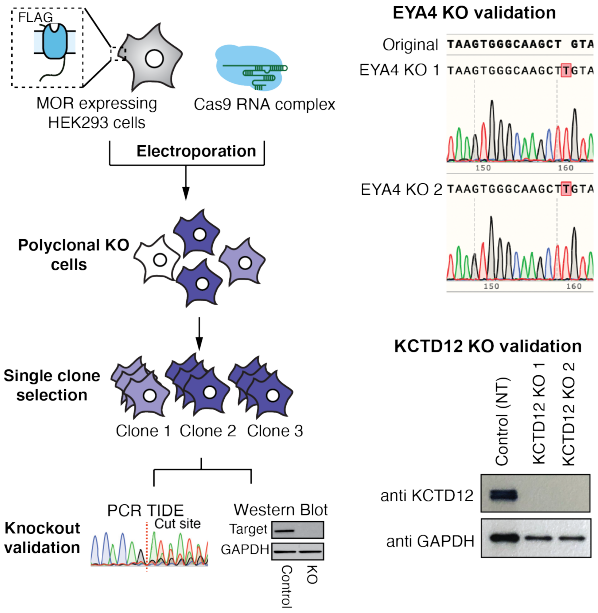

Figure S8. Generation and validation of EYA4 and KCTD12 KO cell lines.
KO was validated by PCR and sequencing (EYA4) or Western blot analysis (KCTD12).

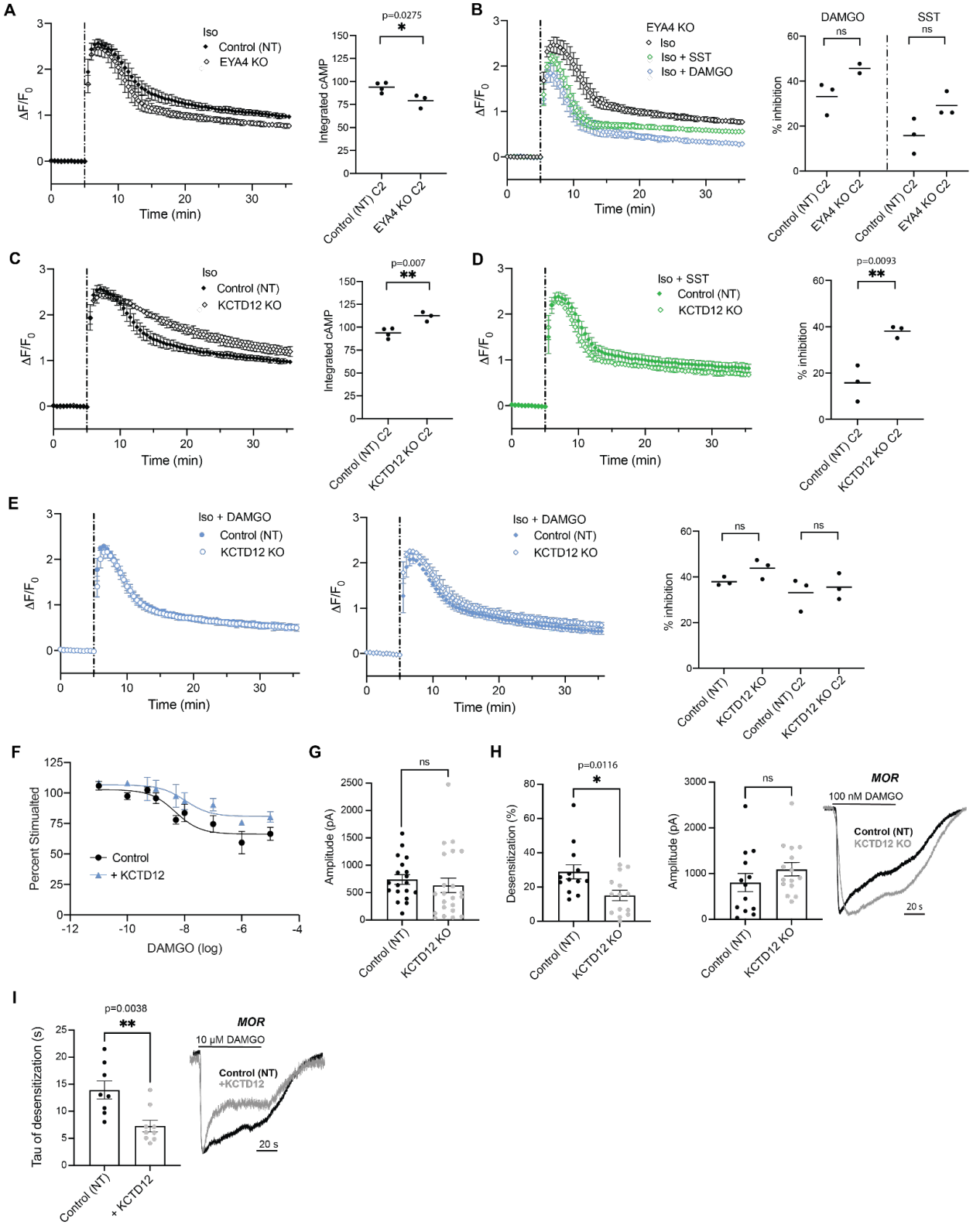

Figure S9. EYA4 and KCTD12 functional validation.

A. cAMP activity in control non-targeting (NT) (closed) and EYA4 KO (open) HEK293 cells stably expressing MOR. Change in fluorescence intensity of cAMP biosensor upon stimulation with 100 nM isoproterenol (Iso) is plotted.
B. cAMP activity EYA4 KO cells upon stimulation with Iso without (black) and with co-application of 1 μM somatostatin (SST, green) or 10 μM DAMGO (blue) is plotted. Iso curve is repeated from panel A.
C. cAMP activity in control (closed) and KCTD12 KO (open) HEK293 cells stably expressing MOR upon stimulation with Iso. Control curve is repeated from panel A.
D. cAMP activity in control and KCTD12 KO cells upon stimulation with Iso and SST. Percent inhibition data for control is repeated from panel B.
E. cAMP activity in control and KCTD12 KO cells upon stimulation with Iso and DAMGO. Clones used in main text figures (circles) and supplemental figures (diamonds) are shown, with the main text control curve repeated from **Figure 5A**. For all cAMP panels, N ≥ 2 and error bars represent standard deviation.
F. cAMP activity in WT cells stably overexpressing MOR-APEX2 and transiently overexpressing KCTD12 or an empty vector control upon stimulation with Iso and DAMGO. N=3 biological replicates with two technical replicates per biological replicate. Error bars represent standard deviation.
G. Summary bar graphs showing the average peak amplitudes of MOR-mediated GIRK currents over 60 s 10 μM DAMGO application, in control and KCTD12 KO HEK cells. Each point represents an individual cell. Error bars represent SEM.
H. Left, summary bar graphs showing the average peak amplitudes and percent desensitization of MOR-mediated GIRK currents over 60 s 100 nM DAMGO, in control and KCTD12 KO HEK cells. Each point represents an individual cell. Unpaired t-test, * p=0.0116. Error bars represent SEM. Right, representative whole cell patch clamp recordings of MOR-mediated GIRK currents in response to 60 s 100 nM DAMGO, in control and KCTD12 KO cells.
I. Left, Quantification of the tau of desensitization of MOR-mediated GIRK currents over 60 s 10 μM DAMGO application, without (control) and with KCTD12 overexpression in HEK 293T cells. Each point represents an individual cell. Unpaired t-test, ** p=0.0038. Error bars represent SEM. Right, representative whole cell patch clamp recordings showing GIRK currents mediated by MOR activation over 60 s 10 μM DAMGO.

Supplemental Tables

Table S1. The table lists all proteins quantified across the MOR-APEX samples and the results of their statistical analysis over the time course of activation with DAMGO, morphine and PZM21.

Table S2. Location specific proteins that were quantified by targeted proteomics in the MOR-APEX samples.

Table S3. Selection of indicative proteins for subcellular location of the receptor from the pairwise comparison of proteins quantified across the spatial references for the plasma membrane (PM-APEX), early endosome (Endo-APEX), and lysosome (Lyso-APEX).

Table S4. The table lists all proteins quantified across the MOR-APEX samples and the results of their statistical analysis over the time course of activation with DAMGO, morphine and PZM21 after detrending of the dataset for location specific effects.

Table S5. Ligand-dependent proximal interaction network of MOR. The table contains all proteins that show a significant fold change for at least one ligand before and after detrending of the data for location-specific effects.

Table S6. Targeted proteomics (SRM) assays used to quantify selected proteins in the MOR-APEX dataset including localization markers and potential interactors of MOR.

References

1. Rask-Andersen, M., Masuram, S. & Schiöth, H. B. The druggable genome: Evaluation of drug targets in clinical trials suggests major shifts in molecular class and indication. *Annu. Rev. Pharmacol. Toxicol.* **54**, 9–26 (2014).
2. Hilger, D., Masureel, M. & Kobilka, B. K. Structure and dynamics of GPCR signaling complexes. *Nat. Struct. Mol. Biol.* **25**, 4–12 (2018).
3. Allen, J. A. & Roth, B. L. Strategies to discover unexpected targets for drugs active at G protein-coupled receptors. *Annu. Rev. Pharmacol. Toxicol.* **51**, 117–144 (2011).
4. Wan, Q. *et al.* Mini G protein probes for active G protein-coupled receptors (GPCRs) in live cells. *J. Biol. Chem.* **293**, 7466–7473 (2018).
5. Olsen, R. H. J. *et al.* TRUPATH, an open-source biosensor platform for interrogating the GPCR transducerome. *Nat. Chem. Biol.* **16**, 841–849 (2020).
6. Peng, G. E., Pessino, V., Huang, B. & von Zastrow, M. Spatial decoding of endosomal cAMP signals by a metastable cytoplasmic PKA network. *Nat. Chem. Biol.* **17**, 558–566 (2021).
7. Stoeber, M. *et al.* Agonist-selective recruitment of engineered protein probes and of GRK2 by opioid receptors in living cells. *Elife* **9**, (2020).
8. Irannejad, R. *et al.* Functional selectivity of GPCR-directed drug action through location bias. *Nat. Chem. Biol.* **13**, 799–806 (2017).
9. Irannejad, R. *et al.* Conformational biosensors reveal GPCR signalling from endosomes. *Nature* **495**, 534–538 (2013).
10. Irannejad, R., Tsvetanova, N. G., Lobingier, B. T. & von Zastrow, M. Effects of endocytosis on receptor-mediated signaling. *Curr. Opin. Cell Biol.* **35**, 137–143 (2015).
11. Stoeber, M. *et al.* A Genetically Encoded Biosensor Reveals Location Bias of Opioid Drug Action. *Neuron* **98**, 963–976.e5 (2018).
12. Tsvetanova, N. G. & von Zastrow, M. Spatial encoding of cyclic AMP signaling specificity by GPCR endocytosis. *Nat. Chem. Biol.* **10**, 1061–1065 (2014).
13. Nash, C. A., Wei, W., Irannejad, R. & Smrcka, A. V. Golgi localized β1-adrenergic receptors stimulate Golgi PI4P hydrolysis by PLCε to regulate cardiac hypertrophy. *Elife* **8**, (2019).
14. Jensen, D. D. *et al.* Neurokinin 1 receptor signaling in endosomes mediates sustained nociception and is a viable therapeutic target for prolonged pain relief. *Sci. Transl. Med.* **9**, (2017).
15. Manglik, A. *et al.* Structure-based discovery of opioid analgesics with reduced side effects. *Nature* **537**, 185–190 (2016).
16. Grim, T. W. *et al.* A G protein signaling-biased agonist at the μ-opioid receptor reverses morphine tolerance while preventing morphine withdrawal. *Neuropsychopharmacology* **45**, 416–425 (2020).
17. DeWire, S. M., Yamashita, D. S., Rominger, D. H. & Liu, G. AG protein-biased ligand at the μ-opioid receptor is potently analgesic with reduced gastrointestinal and respiratory dysfunction compared with morphine. *of Pharmacology and …* (2013).
18. Ramírez-García, P. D. *et al.* A pH-responsive nanoparticle targets the neurokinin 1 receptor in endosomes to prevent chronic pain. *Nat. Nanotechnol.* **14**, 1150–1159 (2019).
19. Jimenez-Vargas, N. N. *et al.* Endosomal signaling of delta opioid receptors is an endogenous mechanism and therapeutic target for relief from inflammatory pain. *Proc. Natl. Acad. Sci. U. S. A.* **117**, 15281–15292 (2020).
20. Jiménez-Vargas, N. N. *et al.* Agonist that activates the μ-opioid receptor in acidified microenvironments inhibits colitis pain without side effects. *Gut* (2021) doi:10.1136/gutjnl-2021-324070.
21. Ehrlich, A. T. *et al.* Biased Signaling of the Mu Opioid Receptor Revealed in Native Neurons. *iScience* **14**, 47–57 (2019).

22. Rhee, H.-W. *et al.* Proteomic mapping of mitochondria in living cells via spatially restricted enzymatic tagging. *Science* **339**, 1328–1331 (2013).
23. Hung, V. *et al.* Proteomic mapping of the human mitochondrial intermembrane space in live cells via ratiometric APEX tagging. *Mol. Cell* **55**, 332–341 (2014).
24. Lobingier, B. T. *et al.* An Approach to Spatiotemporally Resolve Protein Interaction Networks in Living Cells. *Cell* **169**, 350–360.e12 (2017).
25. Paek, J. *et al.* Multidimensional Tracking of GPCR Signaling via Peroxidase-Catalyzed Proximity Labeling. *Cell* **169**, 338–349.e11 (2017).
26. McPherson, J. *et al.* μ-opioid receptors: correlation of agonist efficacy for signalling with ability to activate internalization. *Mol. Pharmacol.* **78**, 756–766 (2010).
27. Lau, E. K. *et al.* Quantitative encoding of the effect of a partial agonist on individual opioid receptors by multisite phosphorylation and threshold detection. *Sci. Signal.* **4**, ra52 (2011).
28. Choi, M. *et al.* MSstats: an R package for statistical analysis of quantitative mass spectrometry-based proteomic experiments. *Bioinformatics* **30**, 2524–2526 (2014).
29. Hegde, R. S., Roychoudhury, K. & Pandey, R. N. The multi-functional eyes absent proteins. *Crit. Rev. Biochem. Mol. Biol.* **55**, 372–385 (2020).
30. Fan, X. *et al.* The alpha subunits of Gz and Gi interact with the eyes absent transcription cofactor Eya2, preventing its interaction with the six class of homeodomain-containing proteins. *J. Biol. Chem.* **275**, 32129–32134 (2000).
31. Embry, A. C., Glick, J. L., Linder, M. E. & Casey, P. J. Reciprocal signaling between the transcriptional co-factor Eya2 and specific members of the Galphai family. *Mol. Pharmacol.* **66**, 1325–1331 (2004).
32. Schwenk, J. *et al.* Native GABA(B) receptors are heteromultimers with a family of auxiliary subunits. *Nature* **465**, 231–235 (2010).
33. Turecek, R. *et al.* Auxiliary GABAB receptor subunits uncouple G protein βγ subunits from effector channels to induce desensitization. *Neuron* **82**, 1032–1044 (2014).
34. Zheng, S., Abreu, N., Levitz, J. & Kruse, A. C. Structural basis for KCTD-mediated rapid desensitization of GABAB signalling. *Nature* **567**, 127–131 (2019).
35. DeWire, S. M. *et al.* A G protein-biased ligand at the μ-opioid receptor is potently analgesic with reduced gastrointestinal and respiratory dysfunction compared with morphine. *J. Pharmacol. Exp. Ther.* **344**, 708–717 (2013).
36. Kliewer, A. *et al.* Morphine-induced respiratory depression is independent of ß-arrestin2 signalling. *Br. J. Pharmacol.* **177**, 2923–2931 (2020).
37. Bachmutsky, I., Wei, X. P., Durand, A. & Yackle, K. ß-arrestin 2 germline knockout does not attenuate opioid respiratory depression. *Elife* **10**, (2021).
38. Muntean, B. S. *et al.* Members of the KCTD family are major regulators of cAMP signaling. *Proc. Natl. Acad. Sci. U. S. A.* **119**, (2022).
39. Cox, J. & Mann, M. MaxQuant enables high peptide identification rates, individualized p.p.b.-range mass accuracies and proteome-wide protein quantification. *Nat. Biotechnol.* **26**, 1367–1372 (2008).
40. Tsai, T.-H. *et al.* Selection of Features with Consistent Profiles Improves Relative Protein Quantification in Mass Spectrometry Experiments. *Mol. Cell. Proteomics* **19**, 944–959 (2020).
41. Yu, G., Wang, L.-G., Han, Y. & He, Q.-Y. clusterProfiler: an R package for comparing biological themes among gene clusters. *OMICS* **16**, 284–287 (2012).
42. Korotkevich, G. *et al.* Fast gene set enrichment analysis. *bioRxiv* (2016) doi:10.1101/060012.
43. MacLean, B. *et al.* Skyline: an open source document editor for creating and analyzing targeted proteomics experiments. *Bioinformatics* **26**, 966–968 (2010).
44. Vizcaíno, J. A. *et al.* 2016 update of the PRIDE database and its related tools. *Nucleic Acids Res.* **44**, 11033 (2016).

45. Sharma, V. *et al.* Panorama: a targeted proteomics knowledge base. *J. Proteome Res.* **13**, 4205–4210 (2014).
46. Choi, H. *et al.* SAINT: probabilistic scoring of affinity purification-mass spectrometry data. *Nat. Methods* **8**, 70–73 (2011).
47. Sowa, M. E., Bennett, E. J., Gygi, S. P. & Harper, J. W. Defining the human deubiquitinating enzyme interaction landscape. *Cell* **138**, 389–403 (2009).
48. Shannon, P. *et al.* Cytoscape: a software environment for integrated models of biomolecular interaction networks. *Genome Res.* **13**, 2498–2504 (2003).
49. Abreu, N., Acosta-Ruiz, A., Xiang, G. & Levitz, J. Mechanisms of differential desensitization of metabotropic glutamate receptors. *Cell Rep.* **35**, 109050 (2021).
50. Vivaudou, M. *et al.* Probing the G-protein regulation of GIRK1 and GIRK4, the two subunits of the KACh channel, using functional homomeric mutants. *J. Biol. Chem.* **272**, 31553–31560 (1997).